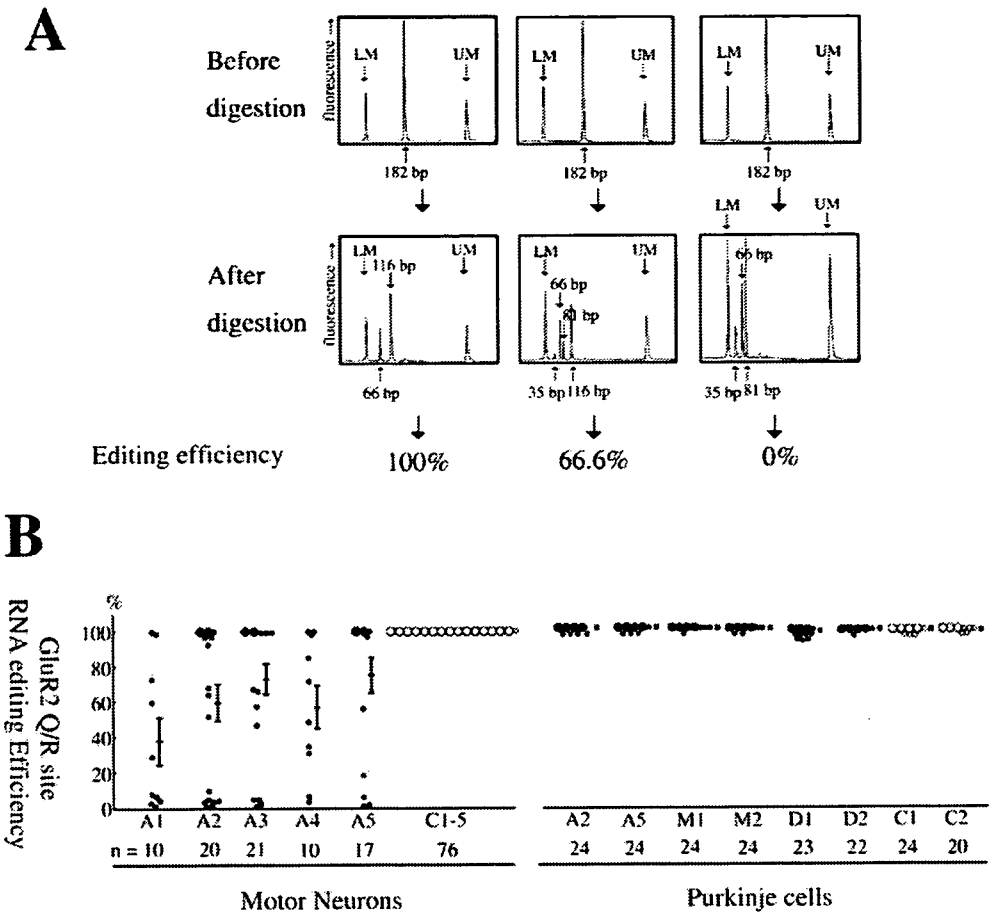

Fig. 5 A Analysis of RNA editing efficiency: When all of the RT-PCR products are derived from edited GluR2 mRNA, two bands (66 and 116 bp) are detected; by contrast, when all of the RT-PCR products are derived from unedited GluR2, three bands (35, 66, and 81 bp) are detected. When both edited and unedited GluR2 subunits coexist, four bands (35, 66, 81, and 116 bp) are detected. **B** Editing efficiency at the GluR2 Q/R site in single neurons of ALS, disease control and normal control subjects (modified from Fig. 1 in [67]). The editing efficiency varied greatly, from 0% to 100% (mean: 38.1–75.3%), among the motor neurons of each individual with ALS (A1–A5), and was not complete in 44 of them (56%); this was in marked contrast to the control motor neurons (C1–5), of which all 76 examined showed 100% editing efficiency. The editing efficiency in Purkinje cells was virtually complete (greater than 99.8%) in the ALS, disease control (dentatorubral-pallidoluysian atrophyDRPLA (D), multiple system atrophyMSA (M)) and the normal control groups (C)

the endoplasmic reticulum (ER) to the cell surface [71]. Therefore, if the RNA editing were deficient, even in a small proportion, then GluR2Q-containing receptors would be formed preferentially in the endoplasmic reticulumER, and receptors containing GluR2Q and GluR1 or GluR3 would be readily transported to the membrane, resulting in the preferential expression of Ca^{2+}-permeable functional AMPA receptors in the postsynaptic membrane. The effects of GluR2 RNA editing deficiency may be more conspicuous in spinal motor neurons, where the expression level of GluR2 is relatively low compared with that in other neuronal subsets [36]. According to this scheme, a small increase in GluR2Q with deficient GluR2 RNA editing will greatly increase the proportion of GluR2Q-containing, and therefore Ca^{2+}-permeable, functional AMPA receptors, thereby promoting excitotoxicity in ALS motor neurons [47, 48, 50–52].

Editing enzymes and RNA editing of GluR

Enzymes responsible for the A-to-I conversion have been termed "'adenosine deaminases acting on RNA'" (ADARs), and three structurally related ADARs (ADAR1 to ADAR3) have been identified in mammals [72–77]. ADAR1 and ADAR2 are expressed in most tissues [72, 74, 78, 79] and recognize the adenosine residue to be edited through the structure of the duplex that is formed between the editing site and its editing site complementary sequence (ECS), which is located in a downstream intron of the precursor (pre-) mRNA (Fig. 6) [80–82]. ADAR2 predominantly catalyzes RNA editing at the Q/R site of GluR2 both in vivo and in vitro, whereas both ADAR1 and ADAR2 catalyze the Q/R sites of GluR5 and GluR6, which are subunits of kainate receptors [83, 84]. ADAR3 is expressed

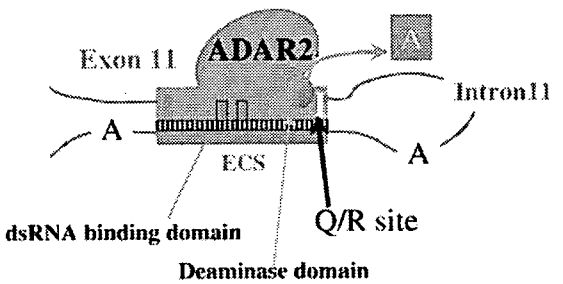

Fig. 6 ADAR2 and RNA editing. ADAR2 has two double-stranded RNA-binding domains (*square*) and one catalytic domain (*cube*), and it recognizes the adenosine residue (*A*) to be edited through the structure of the duplex that is formed between the editing site (e.g., the Q/R site in exon 11 of GluR2 pre-mRNA) and its editing site complementary sequence (*ECS*), which is located in a downstream sequence (e.g., in intron 11 of GluR2 pre-mRNA). Adenosine in the edited site is substituted to inosine (*I*), but adenosine that is not located in the editing site or the ECS remains unedited

exclusively in the brain, but is catalytically inactive on both extended double-stranded RNA and known pre-mRNA editing substrates [75, 77].

In mammalian and human brains, the editing efficiency at each editing position of GluRs is developmentally and regionally regulated [52, 56, 62, 85, 86], and the Q/R sites of GluR5 and GluR6 have been reported to be edited less in white matter than in gray matter [58, 68, 86–91]. By contrast, the GluR2 Q/R site is almost completely edited in various brain regions, including white matter in neonatal and adult rodent brains [56, 87, 92, 93]. GluR2 mRNA in human brains including white matter is, however, not always completely edited at the Q/R site [61, 62, 65, 66, 68, 91, 94, 95]. We have demonstrated an editing efficiency of virtually 100% in single neuron tissues from various neuronal subsets, but a significantly low editing efficiency in adult, but not in immature, human white matter [68, 91]. It seems likely that, in contrast to neurons, human glial cells physiologically express Ca^{2+}-permeable AMPA receptors: oligodendrocytes express those containing unedited GluR2 subunits, and astrocytes and Bergmann's glial cells express those lacking edited GluR2 subunits [23, 96, 97]. Therefore, the regional, and thus presumably cell-specific, regulation of GluR2 Q/R editing might occur in the human central nervous system.

ADAR2

It has been shown that the mRNA expression of ADAR2, the most efficient double-stranded RNA deaminase for editing GluRs, is regulated in a cell-specific manner throughout development and in rodent brain, is first detected by in situ hybridization in the thalamic nuclei formation at embryonic day 19 (E19), with more extensive and widespread distribution by the third postnatal week when the expression is highest in the thalamic nuclei and very low in white matter [98]. Editing efficiency at the editing sites of GluRs have been found to parallel the expression levels of ADAR2 mRNA in developmental rat [86, 87, 99–101] and human [91] brains, in a cultured human teratocarcinoma cell line [102], and in surgically excised hippocampus from patients affected with refractory epilepsy [103].

An association between the level of ADAR2 expression and editing efficiency at the GluR2 Q/R site has been also demonstrated by the observation that an RNA editing efficiency of less than 100% occurred only when the ratio of ADAR2 mRNA to total AMPA receptor subunit (GluR1-GluR4) mRNA was below 20×10^{-3} in human white matter (Fig. 7B) [68]. No such correlation was observed between the editing efficiency at GluR2 mRNA and the ratio of ADAR1 mRNA to total GluR mRNA, or between the editing efficiency at GluR5 or GluR6 mRNA and the ratio of either ADAR1 or ADAR2 mRNA to total GluR mRNA (Fig. 7A) [68]. Our results on human brain are in agreement with in vivo and in vitro evidence obtained in animal brains, indicating that ADAR2 predominantly catalyzes RNA editing at the Q/R site of GluR2 [55, 74, 78, 83, 104, 105], whereas the Q/R sites of GluR5 and GluR6 are edited not only by ADAR2 but also by ADAR1 [74, 75, 78, 81, 83, 84].

Taken together, the expression level of ADAR2 mRNA is one factor determining the editing efficiency of GluR2 at the Q/R site, although the nonlinear correlation suggests that another factor or factors may be also involved in the regulation of editing activity. Indeed, inhibitors of ADARs have been identified as sequence-nonspecific double-stranded RNA-binding proteins in *Xenopus* oocytes [106].

Significance of GluR2 underediting

GluR2 Q/R site editing in neurons occurs with virtually 100% efficiency throughout life from an embryonic stage, and the early demise of mice deficient in GluR2 RNA editing caused by neuronal death [30] can be rescued by restoring RNA editing [84], indicating that GluR2 modification by RNA editing is a biologically crucial event for neuronal survival and its deficiency is a direct cause of neuronal death. Thus, marked reduction of RNA editing in ALS motor neurons [67] may be a direct cause of the selective motor neuron death seen in ALS.

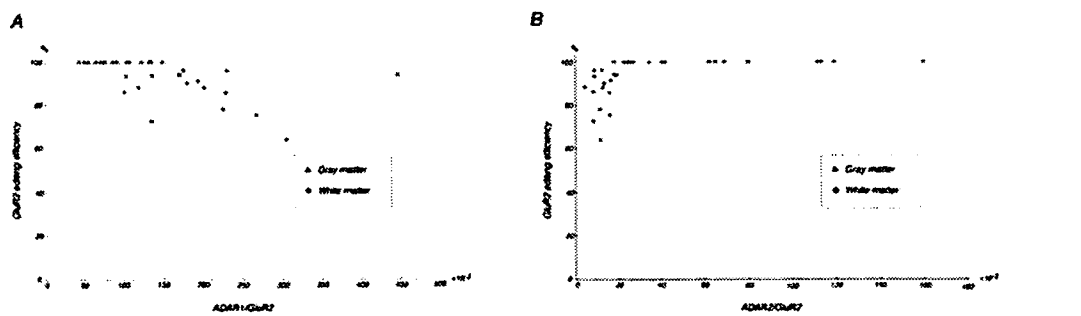

Fig. 7 Relationship between editing efficiency at the Q/R site of GluR2 and the abundance of ADAR1 mRNA (**A**) or ADAR2 mRNA (**B**) relative to GluR2 mRNA. **A** No relationship is found between GluR2 editing and the expression of ADAR1 mRNA relative to GluR2 mRNA. **B** In samples where the abundance of ADAR2 mRNA relative to GluR2 mRNA is less than 20×10^{-3}, GluR2 is not completely edited. By contrast, when the relative abundance is greater than 20×10^{-3}, GluR2 is completely edited. *Cbl*, Cerebellum; *BW*, cerebellar white matter; *Cx*, cerebral cortex; *CW*, cerebral white matter. (Adapted from Fig.7 in [68] with permission)

As mentioned above, AMPA receptors in glial cells seem to be more Ca^{2+}permeable than those in neurons, and a deficiency in RNA editing at the GluR2 Q/R site seems to cause significant cell death only when it occurs in neurons. Therefore, the recent finding of a reduction in GluR2 Q/R editing in malignant gliomas [94] may have different biological significance in comparison to the editing deficiency that occurs in neuronal tissue in ALS [67]. Indeed, the magnitude of the editing efficiency that was observed in malignant gliomas (69–88%) was within the range that we detected in normal white matter (64–99%) [68].

It is likely that the molecular mechanism underlying the deficiency in RNA editing is a reduction in ADAR2 deaminase activity. Our results suggest that the expression level of ADAR2 mRNA is a determining factor in this reduced activity; thus, restoring ADAR2 activity selectively in motor neurons, for example, by transfection of an ADAR2 cDNA construct using a motor neuron-specific vehicle for enhancing ADAR2 mRNA levels may be a specific therapeutic strategy for ALS. With this more focused research target, it is our sincere hope that a specific therapy for ALS will be developed in the near future.

Acknowledgements This study was supported, in part, by a grant from the ALS Association (to S.K.), grants-in-aid for Scientific Research on Priority Areas from the Ministry of Education, Culture, Sports, Science, and Technology of Japan (13210031,14017020, 15016030 to S.K.), a grant from The Nakabayashi Trust for ALS Research (to Y.K.), a grant from The Naito Foundation (to Y.K.), and a grant from the Japan ALS Association (to Y.K.).

References

1. Rosen DR, Siddique T, Patterson D, Figlewicz DA, Sapp P, Hentati A, Donaldson D, Goto J, O'Regan JP, Deng HX et al (1993) Mutations in Cu/Zn superoxide dismutase gene are associated with familial amyotrophic lateral sclerosis. Nature 362:59–62
2. Hadano S, Hand CK, Osuga H, Yanagisawa Y, Otomo A, Devon RS, Miyamoto N, Showguchi-Miyata J, Okada Y, Singaraja R, Figlewicz DA, Kwiatkowski T, Hosler BA, Sagie T, Skaug J, Nasir J, Brown RH Jr, Scherer SW, Rouleau GA, Hayden MR, Ikeda JE (2001) A gene encoding a putative GTPase regulator is mutated in familial amyotrophic lateral sclerosis 2. Nat Genet 29:166–173
3. Yang Y, Hentati A, Deng HX, Dabbagh O, Sasaki T, Hirano M, Hung WY, Ouahchi K, Yan J, Azim AC, Cole N, Gascon G, Yagmour A, Ben-Hamida M, Pericak-Vance M, Hentati F, Siddique T (2001) The gene encoding alsin, a protein with three guanine-nucleotide exchange factor domains, is mutated in a form of recessive amyotrophic lateral sclerosis. Nat Genet 29:160–165
4. Chen YZ, Bennett CL, Huynh HM, Blair IP, Puls I, Irobi J, Dierick I, Abel A, Kennerson ML, Rabin BA, Nicholson GA, Auer-Grumbach M, Wagner K, De Jonghe P, Griffin JW, Fischbeck KH, Timmerman V, Cornblath DR, Chance PF (2004) DNA/RNA Helicase Gene Mutations in a Form of Juvenile Amyotrophic Lateral Sclerosis (ALS4). Am J Hum Genet 74:1128–1135
5. Julien JP (2001) Amyotrophic lateral sclerosis. unfolding the toxicity of the misfolded. Cell 104:581–591
6. Hafezparast M, Klocke R, Ruhrberg C, Marquardt A, Ahmad-Annuar A, Bowen S, Lalli G, Witherden AS, Hummerich H, Nicholson S, Morgan PJ, Oozageer R, Priestley JV, Averill S, King VR, Ball S, Peters J, Toda T, Yamamoto A, Hiraoka Y, Augustin M, Korthaus D, Wattler S, Wabnitz P, Dickneite C, Lampel S, Boehme F, Peraus G, Popp A, Rudelius M, Schlegel J, Fuchs H, Hrabe de Angelis M, Schiavo G, Shima DT, Russ AP, Stumm G, Martin JE, Fisher EM (2003) Mutations in dynein link motor neuron degeneration to defects in retrograde transport. Science 300:808–812
7. Oosthuyse B, Moons L, Storkebaum E, Beck H, Nuyens D, Brusselmans K, Van Dorpe J, Hellings P, Gorselink M, Heymans S, Theilmeier G, Dewerchin M, Laudenbach V, Vermylen P, Raat H, Acker T, Vleminckx V, Van Den Bosch L, Cashman N, Fujisawa H, Drost MR, Sciot R, Bruyninckx F, Hicklin DJ, Ince C, Gressens P, Lupu F, Plate KH, Robberecht W, Herbert JM, Collen D, Carmeliet P (2001) Deletion of the hypoxia-response element in the vascular endothelial growth factor promoter causes motor neuron degeneration. Nat Genet 28:131–138
8. Azzouz M, Ralph GS, Storkebaum E, Walmsley LE, Mitrophanous KA, Kingsman SM, Carmeliet P, Mazarakis ND (2004) VEGF delivery with retrogradely transported lentivector prolongs survival in a mouse ALS model. Nature 429:413–417
9. MacGowan DJ, Scelsa SN, Waldron M (2001) An ALS-like syndrome with new HIV infection and complete response to antiretroviral therapy. Neurology 57:1094–1097
10. Moulignier A, Moulonguet A, Pialoux G, Rozenbaum W (2001) Reversible ALS-like disorder in HIV infection. Neurology 57:995–1001
11. Rothstein JD, Martin LJ, Kuncl RW (1992) Decreased glutamate transporter by the brain and spinal cord in amyotrophic lateral sclerosis. N Engl J Med 326:1464–1468
12. Rothstein JD, Van Kammen M, Levey AI, Martin LJ, Kuncl R, W. (1995) Selective loss of glial glutamate transporter GLT-1 in amyotrophic lateral sclerosis. Ann Neurol 38:73–84
13. Nagai M, Abe K, Okamoto K, Y. Itoyama (1998) Identification of alternative splicing forms of GLT-1 mRNA in the spinal cord of amyotrophic lateral sclerosis patients. Neurosci Lett 244: 165–168
14. Rothstein JD, Jin L, Dykes-Hoberg M, Kuncl RW (1993) Chronic inhibition of glutamate uptake produces a model of slow neurotoxicity. Proc Natl Acad Sci USA 90:6591–6595
15. Vandenberghe W, Ihle EC, Patneau DK, Robberecht W, Brorson JR (2000) AMPA receptor current density, not desensitization, predicts selective motoneuron vulnerability. J Neurosci 20:7158–7166
16. Vandenberghe W, Robberecht W, Brorson JR (2000) AMPA receptor calcium permeability, GluR2 expression, and selective motoneuron vulnerability. J Neurosci 20:123–132
17. Kwak S, Nakamura R (1995) Selective degeneration of inhibitory interneurons in the rat spinal cord induced by intrathecal infusion of acromelic acid. Brain Res 702:61–71
18. Kwak S, Nakamura R (1995) Acute and late neurotoxicity in the rat spinal cord in vivo induced by glutamate receptor agonists. J Neurol Sci 129 [Suppl]: 99–103
19. Carriedo SG, Yin HZ, Weiss JH (1996) Motor neurons are selectively vulnerable to AMPA/kainate receptor-mediated injury in vitro. J Neurosci 16:4069–4079
20. Lu YM, Yin HZ, Chiang J, Weiss JH (1996) Ca^{2+}-permeable AMPA/kainate and NMDA channels: high rate of Ca^{2+} influx underlies potent induction of injury. J Neurosci 16:5457–5465
21. Hollmann M, Hartley M, Heinemann S (1991) Ca^{2+} permeability of KA-AMPA-gated glutamate receptor channels depends on subunit composition. Science 252:851–853
22. Verdoorn T, Burnashev N, Monye rH, Seeburg P, Sakmann B (1991) Structural determinants of ion flow through recombinant glutamate receptor channels. Science 252:1715–1718
23. Burnashev N, Monyer H, Seeburg P, Sakmann B (1992) Divalent ion permeability of AMPA receptor channels is dominated by the edited form of a single subunit. Neuron 8:189–198

24. Koh DS, Burnashev N, Jonas P (1995) Block of native Ca (2+)-permeable AMPA receptors in rat brain by intracellular polyamines generates double rectification. J Physiol (Lond) 486: 305–312
25. Hume RI, Dingledine R, Heinemann SF (1991) Identification of a site in glutamate receptor subunits that controls calcium permeability. Science 253:1028–1031
26. Burnashev N, Zhou Z, Neher E, Sakmann B (1995) Fractional calcium currents through recombinant GluR channels of the NMDA, AMPA and kainate receptor subtypes. J Physiol (Lond) 485:403–418
27. Swanson G, Kamboj S, Cull-Candy S (1997) Single-channel properties of recombinant AMPA receptors depend on RNA editing, splice variation, and subunit composition. J Neurosci 17:58–69
28. Iihara K, Joo DT, Henderson J, Sattler R, Taverna FA, Lourensen S, Orser BA, Roder JC, Tymianski M (2001) The influence of glutamate receptor 2 expression on excitotoxicity in Glur2 null mutant mice. J Neurosci 21:2224–2239
29. Jia Z, Agopyan N, Miu P, Xiong Z, Henderson J, Gerlai R, Taverna F, Velumian A, MacDonald J, Carlen P, Abramow-Newerly W, Roder J (1996) Enhanced LTP in mice deficient in the AMPA receptor GluR2. Neuron 17:945–956
30. Brusa R, Zimmermann F, Koh D, Feldmeyer D, Gass P, Seeburg P, Sprengel R (1995) Early-onset epilepsy and postnatal lethality associated with an editing-deficient GluR-B allele in mice. Science 270:1677–1680
31. Feldmeyer D, Kask K, Brusa R, Kornau HC, Kolhekar R, Rozov A, Burnashev N, Jensen V, Hvalby O, Sprengel R, Seeburg PH (1999) Neurological dysfunctions in mice expressing different levels of the Q/R site-unedited AMPAR subunit GluR-B. Nat Neurosci 2:57–64
32. Tomiyama M, Rodriguez-Puertas R, Cortes R, Christnacher A, Sommer B, Pazos A, Palacios JM, Mengod G (1996) Differential regional distribution of AMPA receptor subunit messenger RNAs in the human spinal cord as visualized by in situ hybridization. Neuroscience 75:901–915
33. Virgo L, Samarasinghe S, de Belleroche J (1996) Analysis of AMPA receptor subunit mRNA expression in control and ALS spinal cord. NeuroReport 7:2507–2511
34. Williams T, Day N, Ince P, Kamboj R, Shaw P (1997) Calcium-permeable alpha-amino-3-hydroxy-5-methyl-4-isoxazole propionic acid receptors: a molecular determinant of selective vulnerability in amyotrophic lateral sclerosis. Ann Neurol 42:200–207
35. Bar-Peled O, O'Brien RJ, Morrison JH, Rothstein JD (1999) Cultured motor neurons possess calcium-permeable AMPA/kainate receptors. NeuroReport 10:855–859
36. Kawahara Y, Kwak S, Sun H, Ito K, Hashida H, Aizawa H, Jeong S-Y, Kanazawa I (2003) Human spinal motoneurons express low relative abundance of GluR2 mRNA: an implication for excitotoxicity in ALS. J Neurochem 85:680–689
37. Furuyama T, Kiyama H, Sato K, Park HT, Takagi H, Tohyama J (1993) Region-specific expression of subunits of ionotropic glutamate receptors (AMPA-type, KA-type and NMDA receptors) in the rat spinal cord with special reference to nociception. Mol Brain Res 18:141–151
38. Tölle TR, Berthele A, Zieglgänsberger W, Seeburg PH, Wisden W (1993) The differential expression of 16 NMDA and non-NMDA receptor subunits in the rat spinal cord and in periaqueductal gray. J Neurosci 13:5009–5028
39. Grossman SD, Wolfe BB, Yasuda RP, Wrathall JR (1999) Alterations in AMPA receptor subunit expression after experimental spinal cord contusion injury. J Neurosci 19:5711–5720
40. Laslo P, Lipski J, Nicholson LF, Miles GB, Funk GD (2001) GluR2 AMPA receptor subunit expression in motoneurons at low and high risk for degeneration in amyotrophic lateral sclerosis. Exp Neurol 169:461–471
41. Greig A, Donevan SD, Mujtaba TJ, Parks TN, Rao MS (2000) Characterization of the AMPA-activated receptors present on motoneurons. J Neurochem 74:179–191
42. Dai WM, Egebjerg J, Lambert JD (2001) Characteristics of AMPA receptor-mediated responses of cultured cortical and spinal cord neurones and their correlation to the expression of glutamate receptor subunits, GluR1–4. Br J Pharmacol 132:1859–1875
43. Shi S, Hayashi Y, Esteban JA, Malinow R (2001) Subunit-specific rules governing AMPA receptor trafficking to synapses in hippocampal pyramidal neurons. Cell 105:331–343
44. Passafaro M, Piech V, Sheng M (2001) Subunit-specific temporal and spatial patterns of AMPA receptor exocytosis in hippocampal neurons. Nat Neurosci 4:917–926
45. Gerber AP, Keller W (2001) RNA editing by base deamination: more enzymes, more targets, new mysteries. Trends Biochem Sci 26:376–384
46. Keegan LP, Gallo A, O'Connell MA (2001) The many roles of an RNA editor. Nat Rev Genet 2:869–878
47. Chen SH, Habib G, Yang CY, Gu ZW, Lee BR, Weng SA, Silberman SR, Cai SJ, Deslypere JP, Rosseneu M et al (1987) Apolipoprotein B-48 is the product of a messenger RNA with an organ-specific in-frame stop codon. Science 238:363–366
48. Powell LM, Wallis SC, Pease RJ, Edwards YH, Knott TJ, Scott J (1987) A novel form of tissue-specific RNA processing produces apolipoprotein-B48 in intestine. Cell 50:831–840
49. Skuse GR, Cappione AJ, Sowden M, Metheny LJ, Smith HC (1996) The neurofibromatosis type I messenger RNA undergoes base-modification RNA editing. Nucleic Acids Res 24:478–485
50. Sommer B, Köhler M, Sprengel R, Seeberg P (1991) RNA editing in brain controls a determinant of ion flow in glutamate-gated channels. Cell 67:11–19
51. Köhler M, Burnashev N, Sakmann B, Seeburg P (1993) Determinants of Ca^{2+} permeability in both TM1 and TM2 of high affinity kainate receptor channels: diversity by RNA editing. Neuron 10:491–500
52. Lomeli H, Mosbacher J, Melcher T, Hoger T, Geiger JR, Kuner T, Monyer H, Higuchi M, Bach A, Seeburg PH (1994) Control of kinetic properties of AMPA receptor channels by nuclear RNA editing. Science 266:1709–1713
53. Burns CM, Chu H, Rueter SM, Hutchinson LK, Canton H, Sanders-Bush E, Emeson RB (1997) Regulation of serotonin-2C receptor G-protein coupling by RNA editing. Nature 387: 303–308
54. Hoopengardner B, Bhalla T, Staber C, Reenan R (2003) Nervous system targets of RNA editing identified by comparative genomics. Science 301:832–836
55. Rueter SM, Dawson TR, Emeson RB (1999) Regulation of alternative splicing by RNA editing. Nature 399:75–80
56. Burnashev N, Khodorova A, Jonas P, Helm P, Wisden W, Monyer H, Seeburg P, Sakmann B (1992) Calcium-permeable AMPA-kainate receptors in fusiform cerebellar glial cells. Science 256:1566–1570
57. Jonas P, Burnashev N (1995) Molecular mechanisms controlling calcium entry through AMPA-type glutamate receptor channels. Neuron 15:987–990
58. Puchalski R, Louis J, Brose N, Traynelis S, Egebjerg J, Kukekov V, Wenthold R, Rogers S, Lin F, Moran Tea (1994) Selective RNA editing and subunit assembly of native glutamate receptors. Neuron 13:131–147
59. Swanson GT, Feldmeyer D, Kaneda M, Cull-Candy SG (1996) Effect of RNA editing and subunit co-assembly single-channel properties of recombinant kainate receptors. J Physiol (Lond) 492:129–142
60. Pellegrini-Giampietro DE, Gorter JA, Bennett MV, Zukin RS (1997) The GluR2 (GluR-B) hypothesis: Ca (2+)-permeable AMPA receptors in neurological disorders. Trends Neurosci 20:464–470
61. Akbarian S, Smith M, Jones E (1995) Editing for an AMPA receptor subunit RNA in prefrontal cortex and striatum in Alzheimer's disease, Huntington's disease and schizophrenia. Brain Res 699:297–304
62. Paschen W, Hedreen J, Ross C (1994) RNA editing of the glutamate receptor subunits GluR2 and GluR6 in human brain tissue. J Neurochem 63:1596–1602

63. Pellegrini-Giampietro DE, Bennett MV, Zukin RS (1994) AMPA/kainate receptor gene expression in normal and Alzheimer's disease hippocampus. Neuroscience 61:41–49
64. Rump A, Sommer C, Gass P, Bele S, Meissner D, Kiessling M (1996) Editing of GluR2 RNA in the gerbil hippocampus after global cerebral ischemia. J Cerebral Blood Flow Metabol 16:1362–1365
65. Kamphuis W, Lopes da Silva F (1995) Editing status at the Q/R site of glutamate receptor-A, -B, -5 and −6 subunit mRNA in the hippocampal kindling model of epilepsy. Mol Brain Res 29:35–42
66. Takuma H, Kwak S, Yoshizawa T, Kanazawa I (1999) Reduction of GluR2 RNA editing, a molecular change that increases calcium influx through AMPA receptors, selective in the spinal ventral gray of patients with amyotrophic lateral sclerosis. Ann Neurol 46:806–815
67. Kawahara Y, Ito K, Sun H, Aizawa H, Kanazawa I, Kwak S (2004) RNA editing and death of motor neurons. Nature 427:801
68. Kawahara Y, Ito K, Sun H, Kanazawa I, Kwak S (2003) Low editing efficiency of GluR2 mRNA is associated with a low relative abundance of ADAR2 mRNA in white matter of normal human brain. Eur J Neurosci 18:23–33
69. Suzuki T, Tsuzuki K, Kameyama K, Kwak S (2003) Recent advances in the study of AMPA receptors. Folia Pharmacol Jpn 122:515–526
70. Greger IH, Khatri L, Kong X, Ziff EB (2003) AMPA receptor tetramerization is mediated by Q/R editing. Neuron 40:763–774
71. Greger IH, Khatri L, Ziff EB (2002) RNA editing at Arg607 controls AMPA receptor exit from the endoplasmic reticulum. Neuron 34:759–772
72. Kim U, Wang Y, Sanford T, Zeng Y, Nishikura K (1994) Molecular cloning of cDNA for double-stranded RNA adenosine deaminase, a candidate enzyme for nuclear RNA editing. Proc Natl Acad Sci U S A 91:11457–11461
73. O'Connell MA, Krause S, Higuchi M, Hsuan JJ, Totty NF, Jenny A, Keller W (1995) Cloning of cDNAs encoding mammalian double-stranded RNA-specific adenosine deaminase. Mol Cell Biol 15:1389–1397
74. Melcher T, Maas S, Herb A, Sprengel R, Seeburg P, Higuchi M (1996) A mammalian RNA editing enzyme. Nature 379:460–464
75. Melcher T, Maas S, Herb A, Sprengel R, Higuchi M, Seeburg PH (1996) RED2, a brain-specific member of the RNA-specific adenosine deaminase family. J Biol Chem 271:31795–31798
76. O'Connell MA, Gerber A, Keller W (1997) Purification of human double-stranded RNA-specific editase 1 (hRED1) involved in editing of brain glutamate receptor B pre-mRNA. J Biol Chem 272:473–478
77. Chen CX, Cho DS, Wang Q, Lai F, Carter KC, Nishikura K (2000) A third member of the RNA-specific adenosine deaminase gene family, ADAR3, contains both single- and double-stranded RNA binding domains. RNA 6:755–767
78. Lai F, Chen C, Carter K, Nishikura K (1997) Editing of glutamate receptor B subunit ion channel RNAs by four alternatively spliced DRADA2 double-stranded RNA adenosine deaminases. Mol Cell Biol 17:2413–2424
79. Gerber A, O'Connell M, Keller W (1997) Two forms of human double-stranded RNA-specific editase 1 (hRED1) generated by the insertion of an Alu cassette. RNA 3:453–463
80. Higuchi M, Single F, Kohler M, Sommer B, Sprengel R, Seeburg P (1993) RNA editing of AMPA receptor subunit GluR-B: a base-paired intron-exon structure determines position and efficiency. Cell 75:1361–1370
81. Herb A, Higuchi M, Sprengel R, Seeburg PH (1996) Q/R site editing in kainate receptor GluR5 and GluR6 pre-mRNAs requires distant intronic sequences. Proc Natl Acad Sci U S A 93:1875–1880
82. Aruscavage PJ, Bass BL (2000) A phylogenetic analysis reveals an unusual sequence conservation within introns involved in RNA editing. RNA 6:257–269
83. Wang Q, Khillan J, Gadue P, Nishikura K (2000) Requirement of the RNA editing deaminase ADAR1 gene for embryonic erythropoiesis. Science 290:1765–1768
84. Higuchi M, Maas S, Single FN, Hartner J, Rozov A, Burnashev N, Feldmeyer D, Sprengel R, Seeburg PH (2000) Point mutation in an AMPA receptor gene rescues lethality in mice deficient in the RNA-editing enzyme ADAR2. Nature 406:78–81
85. Bernard A, Khrestchatisky M (1994) Assessing the extent of RNA editing in the TMII regions of GluR5 and GluR6 kainate receptors during rat brain development. J Neurochem 62:2057–2060
86. Paschen W, Djuricic B (1994) Extent of RNA editing of glutamate receptor subunit GluR5 in different brain regions of the rat. Cell Mol Neurobiol 14:259–270
87. Paschen W, Djuricic B (1995) Regional differences in the extent of RNA editing of the glutamate receptor subunits GluR2 and GluR6 in rat brain. J Neurosci Methods 56:21–29
88. Garcia-Barcina JM, Matute C (1996) Expression of kainate-selective glutamate receptor subunits in glial cells of the adult bovine white matter. Eur J Neurosci 8:2379–2387
89. de Zulueta MP de, Matute C (1999) Reduced editing of low-affinity kainate receptor subunits in optic nerve glial cells. Brain Res Mol Brain Res 73:104–109
90. Lowe D, Jahn K, Smith D (1997) Glutamate receptor editing in the mammalian hippocampus and avian neurons. Brain Res Mol Brain Res 48:37–44
91. Kawahara Y, Ito K, Sun H, Ito M, Kanazawa I, Kwak S (2004) Regulation of glutamate receptor RNA editing and ADAR mRNA expression in developing human normal and Down's syndrome brains. Brain Res Dev Brain Res 148:151–155
92. Carlson NG, Howard J, Gahring LC, Rogers SW (2000) RNA editing (Q/R site) and flop/flip splicing of AMPA receptor transcripts in young and old brains. Neurobiol Aging 21:599–606
93. Seeburg PH (2002) A-to-I editing: new and old sites, functions and speculations. Neuron 35:17–20
94. Maas S, Patt S, Schrey M, Rich A (2001) Underediting of glutamate receptor GluR-B mRNA in malignant gliomas. Proc Natl Acad Sci U S A 98:14687–14692
95. Kortenbruck G, Berger E, Speckmann EJ, Musshoff U (2001) RNA editing at the Q/R site for the glutamate receptor subunits GLUR2, GLUR5, and GLUR6 in hippocampus and temporal cortex from epileptic patients. Neurobiol Dis 8:459–468
96. Seifert G, Steinhauser C (1995) Glial cells in the mouse hippocampus express AMPA receptors with an intermediate Ca^{2+} permeability. Eur J Neurosci 7:1872–1881
97. Geiger JR, Melcher T, Koh DS, Sakmann B, Seeburg PH, Jonas P, Monyer H (1995) Relative abundance of subunit mRNAs determines gating and Ca^{2+} permeability of AMPA receptors in principal neurons and interneurons in rat CNS. Neuron 15:193–204
98. Paupard MC, O'Connell MA, Gerber AP, Zukin RS (2000) Patterns of developmental expression of the RNA editing enzyme rADAR2. Neuroscience 95:869–879
99. Schmitt J, Dux E. Gissel C, Paschen W (1996) Regional analysis of developmental changes in the extent of GluR6 mRNA editing in rat brain. Brain Res Dev Brain Res 91:153–157
100. Bernard A, Ferhat L, Dessi F, Charton G, Represa A, Ben-Ari Y, Khrestchatisky M (1999) Q/R editing of the rat GluR5 and GluR6 kainate receptors in vivo and in vitro: evidence for independent developmental, pathological and cellular regulation. Eur J Neurosci 11:604–616
101. Paschen W, Dux E, Djuricic B (1994) Developmental changes in the extent of RNA editing of glutamate receptor subunit GluR5 in rat brain. Neurosci Lett 174:109–112
102. Lai F, Chen CX, Lee VM, Nishikura K (1997) Dramatic increase of the RNA editing for glutamate receptor subunits during terminal differentiation of clonal human neurons. J Neurochem 69:43–52

103. Grigorenko EV, Bell WL, Glazier S, Pons T, Deadwyler S (1998) Editing status at the Q/R site of the GluR2 and GluR6 glutamate receptor subunits in the surgically excised hippocampus of patients with refractory epilepsy. NeuroReport 9: 2219–2224
104. Dabiri GA, Lai F, Drakas RA, Nishikura K (1996) Editing of the GLuR-B ion channel RNA in vitro by recombinant double-stranded RNA adenosine deaminase. EMBO J 15:34–45
105. Yang J, Sklar P, Axel R, Maniatis T (1997) Purification and characterization of a human RNA adenosine deaminase for glutamate receptor B pre-mRNA editing. Proc Natl Acad Sci USA 94:4354–4359
106. Saccomanno L, Bass BL (1994) The cytoplasm of Xenopus oocytes contains a factor that protects double-stranded RNA from adenosine-to-inosine modification. Mol Cell Biol 14: 5425–5432

Journal of Neurochemistry, 2007, **102**, 1497–1505 doi:10.1111/j.1471-4159.2007.04534.x

Heat-shock protein 105 interacts with and suppresses aggregation of mutant Cu/Zn superoxide dismutase: clues to a possible strategy for treating ALS

Hirofumi Yamashita,*,† Jun Kawamata,* Katsuya Okawa,‡ Rie Kanki,* Tomoki Nakamizo,* Takumi Hatayama,§ Koji Yamanaka,† Ryosuke Takahashi* and Shun Shimohama*,¶

**Department of Neurology, Kyoto University Graduate School of Medicine, Kyoto, Japan*

†Yamanaka Research Unit, RIKEN Brain Science Institute, Wako, Japan

‡Horizontal Medical Research Organization, Kyoto University Graduate School of Medicine, Kyoto, Japan

§Department of Biochemistry, Kyoto Pharmaceutical University, Kyoto, Japan

¶Department of Neurology, Sapporo Medical University School of Medicine, Sapporo, Japan

Abstract

A dominant mutation in the gene for copper-zinc superoxide dismutase (SOD1) is the most frequent cause of the inherited form of amyotrophic lateral sclerosis. Mutant SOD1 provokes progressive degeneration of motor neurons by an unidentified acquired toxicity. Exploiting both affinity purification and mass spectrometry, we identified a novel interaction between heat-shock protein 105 (Hsp105) and mutant SOD1. We detected this interaction both in spinal cord extracts of mutant $SOD1^{G93A}$ transgenic mice and in cultured neuroblastoma cells. Expression of Hsp105, which is found in mouse motor neurons, was depressed in the spinal cords of $SOD1^{G93A}$ mice as disease progressed, while levels of expression of two other heat-shock proteins, Hsp70 and Hsp27, were elevated. Moreover, Hsp105 suppressed the formation of mutant SOD1-containing aggregates in cultured cells. These results suggest that techniques that raise levels of Hsp105 might be promising tools for alleviation of the mutant SOD1 toxicity.

Keywords: amyotrophic lateral sclerosis, Cu/Zn superoxide dismutase (or superoxide dismutase 1), heat-shock protein 105.

J. Neurochem. (2007) **102**, 1497–1505.

Amyotrophic lateral sclerosis (ALS) is an adult-onset neurodegenerative disease causing the selective loss of motor neurons, which results in progressive and ultimately fatal paralysis of skeletal muscles. Death usually occurs within 2–5 years after onset of the disease and is related to respiratory-muscle weakness. Ten percent of cases of ALS are inherited, and the most frequent cause of inherited ALS is dominant mutations in the gene for Cu/Zn superoxide dismutase (SOD1). More than 100 different mutations in SOD1 have been identified, all of which provoke uniform disease phenotype that is similar to the phenotype of the sporadic disease. Transgenic mice and rats expressing a mutant human gene for SOD1 develop an ALS phenotype, although deletion of SOD1 from mice does not cause motor neuron disease, providing evidence for acquired toxicity due to mutant SOD1 (Bendotti and Carri 2004; Bruijn *et al.* 2004).

Several hypotheses have been proposed to explain the mechanism of mutant SOD1-mediated toxicity, including formation of protein aggregates due to reduced conformational stability, mitochondrial dysfunction, excitotoxicity, abnormal axonal transport, mutant-derived oxidative damage, lack of growth factors, and inflammation. However, the exact mechanism responsible for motor neuron degeneration remains unknown. One plausible hypothesis is linked to the

Received November 30, 2006; revised manuscript received February 08, 2007; accepted February 14, 2007.

Address correspondence and reprint requests to Dr Shun Shimohama, Department of Neurology, Sapporo Medical University School of Medicine, S1 W16, Chuo-ku, Sapporo 060-8543, Japan.
E-mail: shimoha@sapmed.ac.jp

Abbreviations used: ALS, amyotrophic lateral sclerosis; HRP, horseradish peroxidase; HEK, human embryonic kidney; HSF, heat shock factor; IP, immunoprecipitation; MALDI-TOF, matrix-assisted laser desorption/ionization time-of-flight; MS, mass spectrometry; PBS, phosphate-buffered saline; SDS–PAGE, sodium dodecyl sulfate–polyacrylamide gel electrophoresis; SOD, superoxide dismutase; WT, wild-type.

impairment of protein-quality control. Accumulation of mutant SOD1 might result in (i) saturation of the protein-folding and protein-degradation machinery that handles mutant proteins and/or (ii) disruption of vital intracellular processes by misfolded, oligomeric species of SOD1. In such cases, it is likely that mutant SOD1 might provoke toxicity through abnormal interactions between mutant SOD1 and other proteins. In this context, identification of proteins that interact with mutant SOD1 might provide clues to the toxic effects of the mutant protein. Mutant but not wild-type (WT) SOD1 has been found to interact with proteins that are involved in protein-quality control, for example, several heat-shock proteins such as Hsp70 (Shinder *et al.* 2001; Okado-Matsumoto and Fridovich 2002), Hsp40, αB-crystallin (Shinder *et al.* 2001), and Hsp27 (Okado-Matsumoto and Fridovich 2002) and E3 ligases such as dorfin (Niwa *et al.* 2002), NEDL1 (Miyazaki *et al.* 2004), and carboxy terminus of the Hsc70-interacting protein (Choi *et al.* 2004; Urushitani *et al.* 2004).

Abnormal expression of heat-shock proteins has been detected in mutant SOD1 mouse models. Increased expression of Hsp70 in mutant SOD1-expressing fibroblasts (Bruening *et al.* 1999) and of Hsp27 (also referred to as Hsp25) in spinal cord lysates of symptomatic $SOD1^{G93A}$ mice (Vleminckx *et al.* 2002) has been reported, but decreased expression of Hsp27 has also been found in motor neurons from symptomatic $SOD1^{G93A}$ mice (Maatkamp *et al.* 2004). Hsp70/Hsc70 were found in aggregates of mutant SOD1 in the motor neurons of symptomatic mutant SOD1 mice (Watanabe *et al.* 2001; Liu *et al.* 2005). These findings support the hypothesis that depletion of chaperone proteins might be responsible for the toxicity of mutant SOD1. Over-expression of Hsp70 in mutant SOD1 mice did not reverse the disease process (Liu *et al.* 2005), whereas activation of heat shock factor (HSF)-1, a transcription factor for heat-shock proteins, by administration of arimoclomol extended the life span of mutant SOD1 mice (Kieran *et al.* 2004). Such observations suggest that modulation of heat-shock responses might be an attractive strategy for treatment of motor neuron disease. Thus, it seems appropriate to elucidate the mechanism(s) of misregulation of heat-shock proteins that is linked to mutant SOD1-mediated toxicity, which remains poorly understood.

To uncover the properties of mutant SOD1 as they relate to protein-quality control, we investigated the proteins that interact with mutant SOD1 by immunoprecipitation (IP) and subsequent mass spectrometric (MS) analysis. We identified heat-shock protein 105 (Hsp105) as a novel mutant SOD1-interacting protein, and we detected this interaction in spinal cord extracts of mutant $SOD1^{G93A}$ transgenic mice. Levels of expression of Hsp105, which is detected in mouse motor neurons, were depressed in the spinal cords of $SOD1^{G93A}$ mice during disease progression, although levels of expression of other heat-shock protein rose. In addition, Hsp105 suppressed the aggregation of mutant SOD1 in cultured cells. Together, our findings indicate that raising levels of Hsp105 may alleviate the mutant SOD1-mediated toxicity.

Materials and methods

Plasmids

The coding region of human WT SOD1 cDNA was cloned into the expression vector pcDNA3.1(+) (Invitrogen, Carlsbad, CA, USA) and various mutations in SOD1 were generated (Oeda *et al.* 2001) by site-directed mutagenesis using a Mutan™-Super Express Km kit (Takara, Otsu, Japan), in accordance with the manufacturer's instruction. Then a FLAG tag was introduced at the carboxyl terminus of SOD1 and its mutant derivatives by PCR. A fragment of cDNA encoding mouse Hsp105 (Yasuda *et al.* 1995) was cloned into the pcDNA4/TO vector (Invitrogen).

Antibodies

The primary antibodies used for immunoblots or IP included anti-SOD1 antibody (Stressgen Biotechnologies, Victoria, BC, Canada), anti-FLAG antibody (M2; Sigma, St Louis, MO, USA), anti-β-actin antibody (Sigma), mouse anti-Hsp105 antibody (BD Biosciences, San Jose, CA, USA), anti-Hsp70 antibody (Santa Cruz Biotechnology, Santa Cruz, CA, USA), anti-Hsp27 antibody (Santa Cruz Biotechnology), and anti-β-galactosidase antibody (Chemicon, Temecula, CA, USA). For immunofluorescence staining, we used rabbit anti-Hsp105 antibody (Stressgen Biotechnologies) and SMI32 antibody (Sternberger Monoclonals, Baltimore, MA, USA). Secondary antibodies for immunoblots were anti-rabbit IgG conjugated with horseradish peroxidase (HRP; GE Healthcare, Piscataway, NJ, USA), anti-mouse IgG conjugated with HRP (GE Healthcare), and anti-goat IgG conjugated with HRP (Santa Cruz Biotechnology).

Culture and transfection of cells

Neuro2A and human embryonic kidney (HEK)293T cells were maintained in Dulbecco's modified Eagle's medium, supplemented with 10% fetal bovine serum, 100 IU/mL penicillin, 100 μg/mL streptomycin, and 2 mmol/L glutamine. Cells were transiently transfected with Lipofectamine™ 2000 (Invitrogen) according to the manufacturer's instruction. After 24 h, cells were harvested and cellular proteins were subjected to IP or immunoblotting.

Transgenic mice

Mutant (B6SJL-TgN [SOD1-G93A] 1Gur) and WT (B6SJL-Tg [SOD1] 2Gur/J) SOD1 transgenic mice were obtained from the Jackson Laboratory (Bar Harbor, ME, USA). Mice were genotyped by PCR with the following sense and antisense primers: 5′-CATCAGCCCTAATCCATCTGA-3′ and 5′-CGCGACTAACAATCAAAGTGA-3′, respectively. Mice were housed and treated in compliance with the 'Guidelines for Animal Experiments' of Kyoto University, Japan.

Preparation of lysates and IP of proteins

Lysates were prepared, on ice, from cells or tissue in lysis buffer (10 mmol/L Tris–HCl, pH 7.8, 1% Nonidet P-40, 0.15 mol/L NaCl, 1 mmol/L EDTA, and 10 μg/mL aprotinin). After centrifugation (21 600 *g*, 30 min, 4°C), the clarified supernatants were used for

subsequent analysis unless specified. Protein concentrations were determined by Bradford's assay (Bio-Rad, Hercules, CA, USA). For IP, aliquots of 600 μg of protein in 1000 μL of lysis buffer were incubated for 12 h at 4°C with protein G-Sepharose (GE Healthcare). Then they were incubated with rabbit anti-SOD1 (3 μg) or mouse anti-FLAG antibodies (8.8 μg) or normal IgG for 1 h. The antibody–antigen complexes were then incubated with 10 μL of protein G-Sepharose for another hour. After immunoprecipitates had been washed five times with 1000 μL of lysis buffer, protein complexes were eluted with 15 μL of sample buffer for sodium dodecyl sulfate–polyacrylamide gel electrophoresis (SDS–PAGE) (0.125 mol/L Tris–HCl, pH 6.8, 4% SDS, 20% glycerol, 20 mmol/L dithiothreitol, and 0.002% bromo phenol blue) and immediately boiled for 5 min. Supernatants, after clarification by centrifugation, were loaded on a 2–15% polyacrylamide gradient gel (PAGmini; Daiichi Pure Chemicals, Tokyo, Japan) for SDS–PAGE.

Immunoblotting

Lysates prepared in lysis buffer or the whole tissue homogenates, which were prepared by homogenization of spinal cord with the equal volume of SDS sample buffer, were fractionated with SDS–PAGE, then transferred to a polyvinylidene difluoride membrane (Millipore Corporation, Bedford, MA, USA). Membranes were incubated with primary antibodies and appropriate HRP-conjugated secondary antibodies. Immunoreactive proteins on membranes were visualized with the enhanced chemiluminescence western blotting detection reagents (GE Healthcare).

MS

Proteins were identified by MS as described previously (Jensen *et al.* 1996). In brief, after SDS–PAGE, proteins were visualized by silver staining (PlusOne; GE Healthcare) and bands of proteins were excised from gels. After overnight in-gel digestions at 37°C of proteins with trypsin in a buffer that contained 50 mmol/L ammonium bicarbonate (pH 8.0) and 2% acetonitrile, molecular-mass analysis of tryptic peptides was performed by matrix-assisted laser desorption/ionization time-of-flight MS (MALDI-TOF/MS) with an Ultraflex MALDI-TOF/TOF system (Bruker Daltonics, Billerica, MA, USA). The acquired mass spectral data were queried against the National Center for Biotechnology Information non-redundant database using the Mascot (Matrix Science, London, UK) search engine with a peptide mass tolerance of 0.15 Da and allowance for up to two trypsin miscleavages.

Filter trap assay

Filtration of lysates through a cellulose acetate membrane (0.2-μm pores; Advantec, Dublin, CA, USA) was performed with a 96-well dot-blot apparatus (Bio-Rad) as described previously (Wang *et al.* 2002a) with minor modifications. In brief, HEK293T cells were cultured on 35-mm dishes to 70–80% confluence. Cells were co-transfected with 0.6 μg of empty vector or of plasmids encoding LacZ or Hsp105, together with 1 μg of plasmid encoding SOD1^{G93A}-FLAG. After incubation for 48 h, cells were harvested with phosphate-buffered saline (PBS) and briefly sonicated. Lysates were centrifuged at 800 *g* for 10 min at 4°C and the concentrations of proteins in the supernatants were determined. Aliquots of 200 μg of protein in 400 μL of lysis buffer (PBS, 1% SDS) were gently vacuum-filtered through a membrane. Membranes were washed twice with tris-buffered saline-0.05% Tween20 and analyzed by immunoblotting.

Immunofluorescence staining

For immunofluorescence staining, mice were deeply anesthetized with pentobarbital and perfused transcardially with 4% *p*-formaldehyde in PBS. The lumbar spinal cord was dissected out, fixed overnight in 4% *p*-formaldehyde in PBS, and cryoprotected with 30% sucrose in PBS before freezing. Ten-micron cryosections were mounted on slides. After blocking with blocking buffer (5% normal goat serum and 0.3% Triton X-100 in PBS) for half an hour at 25°C, the sections were incubated overnight at 4°C with a mixture of mouse SMI32 antibody (1 : 4000) and rabbit anti-Hsp105 antibody (1 : 100). Bound antibodies were detected with Alexa Fluor 488-conjugated anti-rabbit IgG and Alexa Fluor 594-conjugated anti-mouse IgG antibodies (1 : 1000; Molecular Probes, Eugene, OR, USA). Double-immunostained fluorescent images were recorded with a Leica DMRXA2 confocal microscope (Leica, Wetzlar, Germany).

Statistical analysis

Signals on films were quantified with NIH image software (National Institutes of Health, Bethesda, MD, USA). Statistical significance was assessed by one-way ANOVA followed by Scheffe's *post hoc* test using the KaleidaGraph program (Synergy Software, Reading, PA, USA). Statistical significance was set at a probability value of less than 0.05.

Results

Identification of proteins that interact with mutant SOD1 in Neuro2A cells by MALDI-TOF/MS

We attempted to identify proteins that interact specifically with ALS-associated mutant SOD1 proteins by IP and subsequent MS analysis, as illustrated in Fig. 1a. We transfected Neuro2A cells transiently with plasmids that encoded SOD1^{WT}-FLAG, SOD1^{G85R}-FLAG, or SOD1^{G93A}-FLAG. After 24 h, proteins in lysates from transfected Neuro2A cells were immunoprecipitated with anti-FLAG antibody or control mouse IgG. The immunoprecipitates were fractionated by SDS–PAGE, which was followed by silver staining (Figs 1b and c). We considered all bands in lanes 1, 5, and 6 to represent non-specifically interacting proteins, as they were generated in the absence of mutant SOD1 (lane 1), in the presence of control IgG (lane 5), or in the absence of antibody for IP (lane 6). We detected bands of a protein of ~19 kDa in lanes 2 and 4 and of a protein of ~18 kDa in lane 3, each of which was confirmed to be exogenous SOD1-FLAG by immunoblotting (data not shown). We identified two specific bands of proteins of approximately 70 kDa (p70) and 105 kDa (p105), respectively, that were visualized exclusively in both lanes 3 and 4 (Figs 1b and c). These two bands were excised and subjected to MALDI-TOF/MS analysis. A search for a protein similar to p70 gave 28 matches (*m/z*; 1081.53, 1197.57, 1199.59,

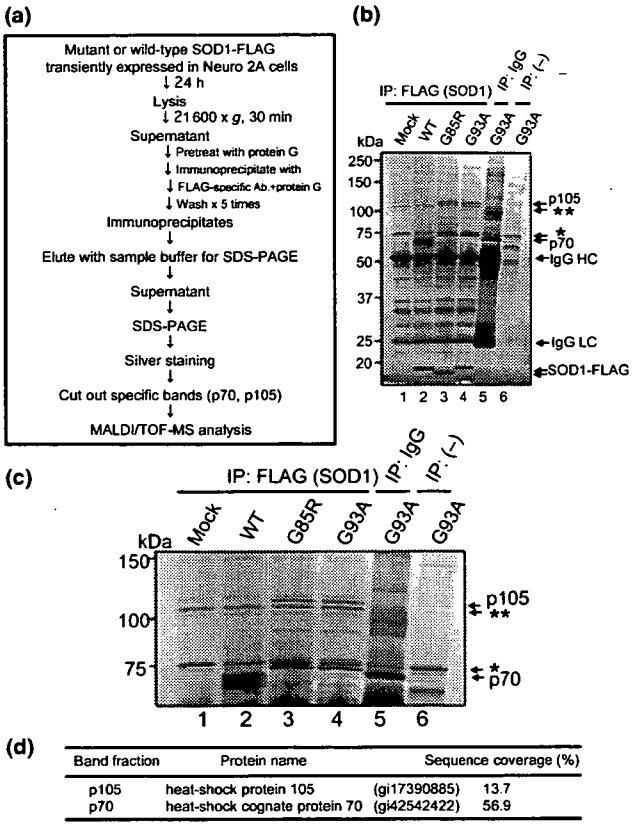

(d)

Band fraction	Protein name		Sequence coverage (%)
p105	heat-shock protein 105	(gi17390885)	13.7
p70	heat-shock cognate protein 70	(gi42542422)	56.9

Fig. 1 Identification of amyotrophic lateral sclerosis-associated mutant superoxide dismutase 1 (SOD1) -interacting proteins by sodium dodecyl sulfate–polyacrylamide gel electrophoresis (SDS–PAGE) and matrix-assisted laser desorption/ionization time-of-flight mass spectrometry (MALDI-TOF/MS) analysis. (a) Scheme for the experiments designed to identify proteins that interact with mutant SOD1. (b and c) Mutant SOD1-interacting proteins, as visualized by silver staining. Arrows indicate interacting proteins (p70 and p105 in lanes 3 and 4), IgG heavy chain (HC), IgG light chain (LC), and FLAG-tagged human SOD1 (lanes 2–4). The G85R mutant form of SOD1 migrates faster than the wild type (lane 3). Asterisks (* and **) denote non-specific bands. Figure 1c shows an enlarged view of the region of the photograph that includes proteins of 50–150 kDa proteins in Fig. 1b. Two proteins that interacted specifically with mutant SOD1 are apparent (p70 and p105; lanes 3 and 4). The mobilities of these correspond to molecular masses of ~70 kDa (p70) and ~105 kDa (p105), respectively. These two bands were excised and were prepared for MS analysis. (d) MS analysis of the excised proteins in Fig. 1c. Percentage sequence coverage of each protein is shown.

1228.55, 1235.54, 1252.59, 1253.56, 1391.67, 1410.62, 1480.71, 1481.77, 1487.67, 1616.76, 1649.78, 1653.81, 1659.84, 1691.73, 1787.97, 1805.86, 1837.97, 1952.04, 1981.99, 2206.09, 2260.13, 2514.34, 2774.37, 2911.63, and 2997.52) with Hsc70 (heat-shock cognate protein 70) with 56.9% sequence coverage. In the analysis of p105, although the sequence coverage (13.7%) was lower than that of p70, 10 peaks of the theoretical mass fingerprint of Hsp105 (heat-shock protein 105) matched with the mass observed (*m/z*; 1133.56, 1321.62, 1388.67, 1479.70, 1481.75, 1487.75, 1562.77, 1637.78, 2035.13, and 2111.03) (Fig. 1d).

Those data highly suggested Hsc70 was interacted with mutant SOD1 proteins as previously reported (Shinder *et al.* 2001). More interestingly, the MS analysis also suggested a novel interaction between Hsp105 and mutant SOD1, which required further confirmation.

Interaction of mutant SOD1 with Hsp105 both in cultured neuroblastoma cells and in mouse spinal cord

Having identified a possible novel interaction between Hsp105 and mutant SOD1, we decided to investigate the role of Hsp105 in the toxicity of mutant SOD1. We first confirmed the interaction between different mutant forms of SOD1 and endogenous Hsp105 in Neuro2A cells. We transiently transfected Neuro2A cells with plasmids that expressed FLAG-tagged SOD1 (WT) and its mutant derivatives (D96N, D90A, G85R, and G93A). Then we immunoprecipitated proteins in lysates with anti-FLAG antibody. Immunoprecipitated proteins were examined by immunoblotting for the presence of Hsp105 (Fig. 2a, upper panel) and SOD1-FLAG (Fig. 2a, second panel). Only G85R and G93A mutant forms of SOD1, which cause motor neuron disease as a dominant trait, interacted with Hsp105; WT SOD1, D96N, and D90A mutant forms of SOD1 did not. The lack of interaction of $SOD1^{D90A}$ and $SOD1^{D96N}$ with Hsp105 suggested the lower toxicity of those mutants. This observation reflects the facts that $SOD1^{D90A}$ causes motor neuron disease as a mainly recessive trait (Andersen *et al.* 1996) and that the D96N mutation has been reported as a non-disease-associated mutation, though controversial (Hand *et al.* 2001; Parton *et al.* 2001).

Next, we used mouse tissue to examine whether the interaction between mutant SOD1 and Hsp105 might occur *in vivo*. Lysates of spinal cord and of liver cells from non-transgenic, $SOD1^{WT}$ and $SOD1^{G93A}$ mice were treated with anti-SOD1 antibody and immunoprecipitates were examined for the presence of Hsp105 (Fig. 2b, upper panel) and SOD1 (Fig. 2b, second panel). In spinal cord extracts, $SOD1^{G93A}$ co-immunoprecipitated with Hsp105 (lane 3), while $SOD1^{WT}$ interacted with Hsp105 at a lower level (lane 2). No evident interaction between SOD1 and Hsp105 was detected in liver, a tissue that is not affected in ALS.

Although it has been reported that Hsp105 is expressed in brain at higher levels (Lee-Yoon *et al.* 1995; Yasuda *et al.* 1995), the cell type(s) that expresses Hsp105 in the spinal cord is unknown. We examined whether Hsp105 is expressed in motor neurons by immunofluorescence staining of spinal cord from non-transgenic mice. Motor neurons that were immunostained with the SMI32 antibody were immunopositive for Hsp105 (Fig. 2c, arrowheads), whereas non-motor neurons were also stained with anti-Hsp105 antibody (Fig. 2c, arrows). Within the motor neurons, Hsp105 was mainly localized in the cytoplasm, as is SOD1.

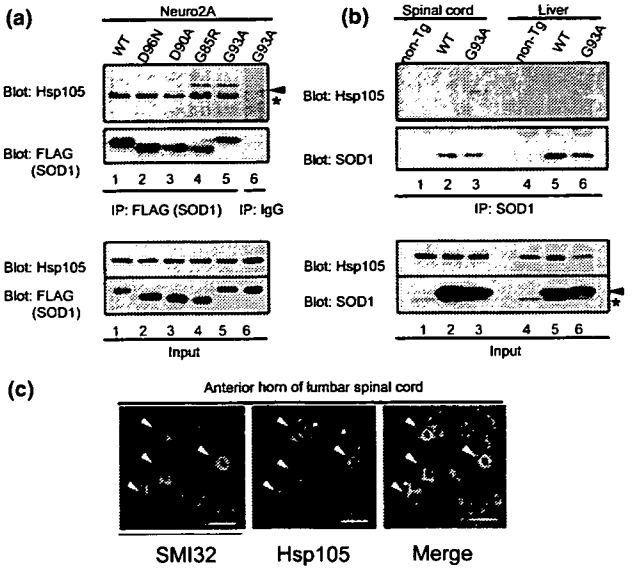

Fig. 2 Hsp105 interacts with mutant superoxide dismutase 1 (SOD1) both in neuroblastoma cells in culture and in mouse spinal cord. (a) Lysates of Neuro2A cells that had been transiently transfected with FLAG-tagged wild-type (WT, lane 1) or mutant SOD1 expression vector (lanes 2–6) were immunoprecipitated with anti-FLAG antibody (lanes 1–5) or normal IgG (lane 6). Immunoprecipitates were analyzed by immunoblotting specific for Hsp105 (top panel) or FLAG (second panel). The arrowhead and the asterisk indicate Hsp105 and non-specific bands, respectively. Ten micrograms (as protein) of each lysate that was subjected to immunoprecipitation were analyzed by immunoblotting (third and fourth panels). (b) Proteins in extracts of spinal cord and of liver from non-transgenic, SOD^{WT}, and SOD^{G93A} mice were immunoprecipitated with anti-SOD1 antibody. Blots were probed for Hsp105 (top panel) or SOD1 (second panel). Eight micrograms (as protein) of the lysate used for immunoprecipitation were immunoblotted with indicated antibodies (third and fourth panels). The arrowhead and the asterisk indicate human SOD1 and endogenous mouse SOD1, respectively. (c) Confocal fluorescence micrographs of lumbar spinal cord from a non-transgenic mouse after double staining with SMI32 antibody (left panel) and anti-Hsp105 antibody (middle panel), and the merged image (right panel). Arrowheads indicate motor neurons that immunoreacted with both antibodies. Arrows indicate non-motor neurons that immunoreacted with only anti-Hsp105 antibody. Hsp105 was mainly localized in the cytoplasm of motor neurons. Scale bars: 50 μm.

Decreased expression of Hsp105 during disease progression in $SOD1^{G93A}$ mice

Heat-shock responses such as increased levels of Hsp27, Hsp70, and Hsp90 have been reported in the spinal cords of mutant SOD1 transgenic mice (Vleminckx *et al.* 2002; Liu *et al.* 2005). To examine changes in levels of heat-shock proteins, including Hsp105, we performed immunoblotting analyses of Hsp105, Hsp70, and Hsp27 in the brain, spinal cord, and liver of SOD^{WT} mice at 5 months of age and in $SOD1^{G93A}$ mice at two different ages. By contrast to levels of other heat-shock proteins, the level of Hsp105 was lower in the spinal cord of symptomatic $SOD1^{G93A}$ mice (4-months old) than in that of pre-symptomatic $SOD1^{G93A}$ mice (2.5-months old) (Fig. 3a, upper panel, lanes 5 and 6).

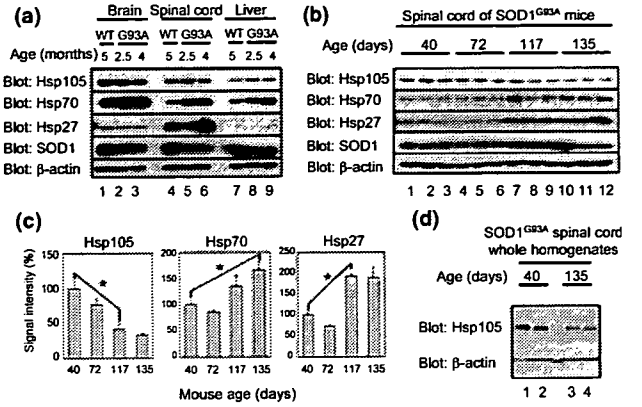

Fig. 3 Decreases in the levels of expression of Hsp105 in the spinal cord during disease progression in superoxide dismutase 1 ($SOD1^{G93A}$) mice. (a) Immunoblotting analysis of Hsp105, Hsp70, and Hsp27 in the brain, spinal cord, and liver of $SOD1^{WT}$ and $SOD1^{G93A}$ mice at two different ages, as indicated. A total of 15 μg of protein was loaded in each lane. The level of Hsp105 was lower in the spinal cord of symptomatic $SOD1^{G93A}$ mice (4 months; lane 6) than in pre-symptomatic $SOD1^{G93A}$ mice (2.5 months; lane 5) (upper panel). The same membrane was immunoprobed for Hsp70 (second panel), Hsp27 (third panel), hSOD1 (fourth panel), and β-actin as a loading control (fifth panel). (b) Immunoblotting analysis of Hsp105, Hsp70, and Hsp27 in the spinal cord of early pre-symptomatic (40-day old), late pre-symptomatic (72-day old), symptomatic (117-day old), and end-stage (135-day old) $SOD1^{G93A}$ mice ($n = 3$ at each time point). A total of 15 μg of protein was loaded in each lane. Membranes were blotted with the indicated antibodies. (c) Densitometric analysis of the immunoblots shown in Fig. 3b. Results are expressed relative to the intensity of signals for 40-day-old mice, which were normalized to 100%. Values are expressed as means ± SE. Asterisks indicate significant difference ($p < 0.05$). (d) Immunoblotting analysis of Hsp105 using whole homogenates from the spinal cord of $SOD1^{G93A}$ mice at pre-symptomatic (40-day old) and end-stage (135-day old). A total of 40 μg of protein was loaded in each lane. Membranes were blotted with the indicated antibodies.

To investigate the level of expression of heat-shock proteins in $SOD1^{G93A}$ mouse spinal cord in grater detail, we performed immunoblotting analysis of Hsp105, Hsp70, and Hsp27 in spinal cords from early pre-symptomatic (40-day old), late pre-symptomatic (72-day old), symptomatic (117-day old), and end-stage (135-day old) $SOD1^{G93A}$ mice (Fig. 3b). Decreased levels of Hsp105 were apparent as early as late pre-symptomatic stage (72 days). However, the decrease did not reach statistical significance. The expression of Hsp105 was significantly depressed as the disease progressed, whereas the levels of expression of both Hsp70 and Hsp27 were elevated at the symptomatic stage and the end-stage (Figs 3b and c). Semi-quantitative immunoblotting confirmed ≈50% decrease of level of Hsp105 in the spinal cord lysates from end-stage $SOD1^{G93A}$ mice (135-day old)

compared with ones from pre-symptomatic mice (40-day old) (Fig. S1).

To investigate whether the decrease in Hsp105 level was associated with the recruitment of Hsp105 to NP-40-insoluble fraction, we performed immunoblotting analysis using whole homogenates from the spinal cord of SOD1^{G93A} mice at pre-symptomatic and end-stage. Whole homogenates were prepared by homogenizing mouse spinal cords with sample buffer for SDS–PAGE and analyzed by immunobloting. The significant decrease in Hsp105 level at end-stage was still observed (Fig. 3d), suggesting that the decrease of Hsp105 was unlikely to be due to the sequestration of Hsp105 into the insoluble fraction.

Inhibition by Hsp105 of the formation of mutant SOD1-containing aggregates in cultured cells

Intracellular inclusions that are strongly immunopositive for SOD1 are found in the motor neurons of mutant SOD1 transgenic mice and in human ALS patients with a mutation in SOD1 (Bruijn *et al.* 1998). These misfolded, detergent-resistant protein aggregates are considered to be relevant to progression of the disease as increased accumulation of these aggregates has been observed in symptomatic mutant SOD1 mice (Bruijn *et al.* 1997; Johnston *et al.* 2000; Wang *et al.* 2002b). To determine whether Hsp105 can suppress the formation of mutant SOD1-containing aggregates, we studied the effects of over-expression of Hsp105 on the aggregation of mutant SOD1 in a filter trap assay. We co-transfected HEK293T cells with an SOD1^{G93A}-FLAG expression vector together with the empty vector, a vector that encoded β-galactosidase or a vector that encoded Hsp105. After 48 h, we harvested the cells and processed them for the filter trap assay. We examined the SDS-insoluble SOD1 aggregates that were retained on cellulose acetate membranes by immunoblotting. Hsp105 significantly suppressed the aggregation of mutant SOD1 (Fig. 4, upper panel). Moreover, the level of expression of SOD1^{G93A} in HEK293T cells was very similar in all the samples examined. Taken together, the results indicate that Hsp105 reduced the level of mutant SOD1-containing aggregates by inhibiting the formation of aggregates rather than by facilitating their degradation.

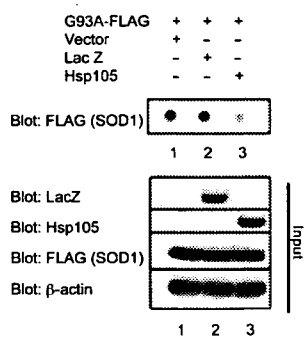

Fig. 4 Hsp105 suppressed the aggregation of mutant superoxide dismutase 1 (SOD1) in cultured cells. HEK293T cells were co-transfected with an SOD1^{G93A}-FLAG expression vector together with the empty vector, an expression vector for β-galactosidase (LacZ), or an expression vector for Hsp105, as indicated. Lysates were analyzed by the filter trap assay with subsequent immunoblotting with anti-FLAG antibody, as described in the text (upper panel). The experiment was repeated three times with essentially the same results. Lower panels show the results of analysis of input in the filter trap assay.

Discussion

In the present study, we have identified a novel interaction between Hsp105 and mutant SOD1 both in cultured cells and in a mouse model. Although the involvement of other heat-shock proteins has been demonstrated in mutant SOD1-mediated toxicity, we demonstrated, for the first time to our knowledge, a decrease in the level of expression of Hsp105, specifically, from the symptomatic to the end-stage of disease in the mutant SOD1 mouse model unlike other heat-shock proteins (Fig. 3). This result might be explained by several properties of Hsp105, which make it uniquely different from Hsp70, a major molecular chaperone that is involved in the folding of newly synthesized and misfolded proteins, even though these heat-shock proteins are structurally similar.

Hsp105, which is a constitutively expressed 105-kDa protein whose synthesis is enhanced by the various stress stimuli, is concentrated in the brain, which suggests a specific role for Hsp105 in stress responses within the nervous system (Lee-Yoon *et al.* 1995; Yasuda *et al.* 1995). Hsp105 exhibits significant homology at the amino acid level to Hsp70, in particular in the amino-terminal ATPase domain. The chaperone activity of Hsp70/Hsc70 (Hsp70s) is controlled by a series of ATP-dependent reaction cycles that consist of the binding of ATP, hydrolysis of ATP, and nucleotide exchange (Buchberger *et al.* 1995; McCarty *et al.* 1995; Rudiger *et al.* 1997). By contrast, Hsp105 does not require ATP to prevent the aggregation of denatured proteins (Yamagishi *et al.* 2003), but it does act as a nucleotide-exchange factor for Hsp70s, which suggests a role for Hsp105 in supporting the functions of Hsp70s (Dragovic *et al.* 2006; Raviol *et al.* 2006). Hsp105 binds to denatured proteins *in vitro* and maintains these proteins in a folding-competent state rather than refolding them itself (Oh *et al.* 1997, 1999; Yamagishi *et al.* 2003). Thus, Hsp105 might function not only in collaboration with Hsp70s but also as a substitute for Hsp70s under severe stress condition, when cellular supplies of ATP have been markedly depleted. In motor neurons that express mutant SOD1, Hsp70s might not be functional, since the level of cellular ATP is likely to be low as a result of consumption by Hsp70s and the ubiquitin-proteasome system. This scenario might explain the failure of over-expression of Hsp70 to mitigate the toxicity of mutant SOD1 in mice (Liu *et al.* 2005). Therefore, rather than

Hsp70, Hsp105 might be a promising candidate for a suppressor of mutant SOD1 toxicity.

We observed the decreased level of Hsp105 in spinal cord of $SOD1^{G93A}$ mice as disease progressed (Fig. 3b) and further confirmed ≈50% decrease in Hsp105 levels at end-stage by semi-quantitative immunoblotting analysis (Fig. S1). This result might partly reflect the loss of motor neurons, which contain abundant Hsp105 proteins. However, considering the facts that lumbar spinal cord sections of $SOD1^{G93A}$ mice at the end-stage show approximately 50% loss of motor neurons (Kostic *et al.* 1997; Bendotti and Carri 2004) and that Hsp105 is expressed not only in motor neurons but also in non-motor neurons (Fig. 2c), it is less likely that Hsp105 was decreased as a consequence of only motor neuronal loss. Immunoblotting analysis of whole spinal cord homogenates also revealed the decreased level of Hsp105 in spinal cord of $SOD1^{G93A}$ mice (Fig. 3d). Therefore, although a fraction of Hsp105 might be lost in aggregates, a significant part of Hsp105 is likely to be consumed or degraded by interacting with mutant SOD1.

Consistent with the reports of the ability of Hsp105 to maintain denatured proteins in a folding-competent state (Oh *et al.* 1997, 1999; Yamagishi *et al.* 2003), we have shown that Hsp105 is able to suppress the formation of aggregates of mutant SOD1 in cultured cells. Mutant SOD1-containing aggregates immunoreact strongly with antibodies raised against ubiquitin, and this phenomenon is common to all mutant SOD1-expressing mouse models (Bruijn *et al.* 1998; Wang *et al.* 2003; Jonsson *et al.* 2004) and human patients (Bruijn *et al.* 1998; Kato *et al.* 2000; Watanabe *et al.* 2001). These findings, together with decreased expression of Hsp105 in symptomatic $SOD1^{G93A}$ mice, suggest that depletion of Hsp105 might contribute to the process of motor neuron degeneration through the accumulation of aggregates of misfolded mutant SOD1.

Hsp105 is essential for cell survival in eukaryotes. Combined deletion in yeast cells of the *SSE1* and *SSE2* genes, which encode members of the Hsp105/110 family, is lethal (Raviol *et al.* 2006). Moreover, recessive mutations in the *SIL1* gene, whose product functions as a nucleotide-exchange factor for the protein of the Hsp70 family, Bip (GRP78), are responsible for Marinesco–Sjögren syndrome, which is characterized by cerebellar atrophy with degeneration of Purkinje and granule cells (Anttonen *et al.* 2005; Senderek *et al.* 2005). Combined with recent reports that Hsp105 is a nucleotide-exchange factor for Hsp70s, these findings provide a link between a functional deficit in a nucleotide-exchange factor for the proteins of the Hsp70 family and neurodegeneration. With respect to neuronal survival, over-expression of Hsp105 has an anti-apoptotic effect in cultured neuronal PC12 cells (Hatayama *et al.* 2001). Hsp105 suppresses apoptosis in a cell culture model of polyglutamine disease, a neurodegenerative disease caused by the toxicity that is derived from a misfolded mutant protein (Ishihara *et al.* 2003). Moreover, we observed Hsp105 prevented caspase-activation induced by proteasomal inhibition with lactacystin in neuroblastoma cell line (Yamashita *et al.*, unpublished data). These results suggest that enhanced expression of Hsp105 might contribute to prevention of motor neuron degeneration through its anti-apoptotic property.

Increased expression of Hsp70s in spinal cord lysates from our $SOD1^{G93A}$ mice and from $SOD1^{G85R}$ mice (Liu *et al.* 2005), together with the impaired heat-shock response of Hsp70 in mutant SOD1-expressing motor neurons (Batulan *et al.* 2003), suggests the enhanced expression of Hsp70s in glial cells. In accordance with this hypothesis, elevated levels of Hsp27 were also observed in the glial cells of $SOD1^{G93A}$ mice (Vleminckx *et al.* 2002). However, this scenario does not apply to Hsp105, because (i) continuous decreases in levels of Hsp105 were observed throughout the course of the disease and (ii) Hsp105 is concentrated in neurons and not in glial cells (Hylander *et al.* 2000). Absence of the induction of expression of Hsp105 in non-neuronal glial cells might exacerbate the toxicity of mutant SOD1 as the toxicity of the mutant protein to motor neurons is non-cell autonomous (Clement *et al.* 2003; Boillee *et al.* 2006).

Over-expression of Hsp70 did not ameliorate the condition of mutant SOD1 mice (Liu *et al.* 2005). By contrast, the pharmacological activation of HSF-1, a transcription factor for heat-shock proteins, extended the life span of mutant SOD1 mice by enhancing the expression of Hsp70s and Hsp90. In the cited study, the level of Hsp105 was not measured (Kieran *et al.* 2004). In spinal and bulbar muscular atrophy mouse model, in which accumulation of misfolded polyglutamine protein causes motor neuron degeneration, pharmacological induction of the expression of HSF-1 by geranylgeranylacetone alleviated polyglutamine-mediated motor neuron disease and activation of HSF-1 was shown to induce the expression of Hsp70, Hsp90, and Hsp105 but not of Hsp27, Hsp40, and Hsp60 (Katsuno *et al.* 2005). In view of our observation of depleted supplies of Hsp105 in $SOD1^{G93A}$ mice, a requirement for enhanced synthesis of Hsp70s, Hsp90, and Hsp105 in both neuronal cells and non-neuronal neighboring cells might be crucial for the mitigation of mutant SOD1-mediated toxicity.

Acknowledgements

The authors thank Dr K. Ishihara (RIKEN Brain Science Institute) for a critical review of the original manuscript, Ms K. Odan (Kyoto University) for technical assistance, and Drs K. Uemura and A. Kuzuya (Kyoto University) for kind advice. This work was supported by the Nakabayashi Trust for ALS Research; the Ministry of Education, Culture, Sports, Science and Technology of Japan; the Ministry of Health, Labor and Welfare of Japan; the Smoking Research Foundation; Philip Morris USA Inc. and Philip Morris International.

Supplementary material

The following supplementary material is available for this article online:

Fig. S1 Semi-quantitative analysis of Hsp105 levels in the spinal cord of SOD1G93A mice.

This material is available as part of the online article from http://www.blackwell-synergy.com.

References

Andersen P. M., Forsgren L., Binzer M. *et al.* (1996) Autosomal recessive adult-onset amyotrophic lateral sclerosis associated with homozygosity for Asp90Ala CuZn-superoxide dismutase mutation. A clinical and genealogical study of 36 patients. *Brain* **119**(Pt. 4), 1153–1172.

Anttonen A. K., Mahjneh I., Hamalainen R. H. *et al.* (2005) The gene disrupted in Marinesco-Sjogren syndrome encodes SIL1, an HSPA5 cochaperone. *Nat. Genet.* **37**, 1309–1311.

Batulan Z., Shinder G. A., Minotti S., He B. P., Doroudchi M. M., Nalbantoglu J., Strong M. J. and Durham H. D. (2003) High threshold for induction of the stress response in motor neurons is associated with failure to activate HSF1. *J. Neurosci.* **23**, 5789–5798.

Bendotti C. and Carri M. T. (2004) Lessons from models of SOD1-linked familial ALS. *Trends Mol. Med.* **10**, 393–400.

Boillee S., Yamanaka K., Lobsiger C. S., Copeland N. G., Jenkins N. A., Kassiotis G., Kollias G. and Cleveland D. W. (2006) Onset and progression in inherited ALS determined by motor neurons and microglia. *Science* **312**, 1389–1392.

Bruening W., Roy J., Giasson B., Figlewicz D. A., Mushynski W. E. and Durham H. D. (1999) Up-regulation of protein chaperones preserves viability of cells expressing toxic Cu/Zn-superoxide dismutase mutants associated with amyotrophic lateral sclerosis. *J. Neurochem.* **72**, 693–699.

Bruijn L. I., Becher M. W., Lee M. K. *et al.* (1997) ALS-linked SOD1 mutant G85R mediates damage to astrocytes and promotes rapidly progressive disease with SOD1-containing inclusions. *Neuron* **18**, 327–338.

Bruijn L. I., Houseweart M. K., Kato S., Anderson K. L., Anderson S. D., Ohama E., Reaume A. G., Scott R. W. and Cleveland D. W. (1998) Aggregation and motor neuron toxicity of an ALS-linked SOD1 mutant independent from wild-type SOD1. *Science* **281**, 1851–1854.

Bruijn L. I., Miller T. M. and Cleveland D. W. (2004) Unraveling the mechanisms involved in motor neuron degeneration in ALS. *Annu. Rev. Neurosci.* **27**, 723–749.

Buchberger A., Theyssen H., Schroder H., McCarty J. S., Virgallita G., Milkereit P., Reinstein J. and Bukau B. (1995) Nucleotide-induced conformational changes in the ATPase and substrate binding domains of the DnaK chaperone provide evidence for interdomain communication. *J. Biol. Chem.* **270**, 16 903–16 910.

Choi J. S., Cho S., Park S. G., Park B. C. and Lee D. H. (2004) Co-chaperone CHIP associates with mutant Cu/Zn-superoxide dismutase proteins linked to familial amyotrophic lateral sclerosis and promotes their degradation by proteasomes. *Biochem. Biophys. Res. Commun.* **321**, 574–583.

Clement A. M., Nguyen M. D., Roberts E. A. *et al.* (2003) Wild-type nonneuronal cells extend survival of SOD1 mutant motor neurons in ALS mice. *Science* **302**, 113–117.

Dragovic Z., Broadley S. A., Shomura Y., Bracher A. and Hartl F. U. (2006) Molecular chaperones of the Hsp110 family act as nucleotide exchange factors of Hsp70s. *EMBO J.* **25**, 2519–2528.

Hand C. K., Mayeux-Portas V., Khoris J., Briolotti V., Clavelou P., Camu W. and Rouleau G. A. (2001) Compound heterozygous D90A and D96N SOD1 mutations in a recessive amyotrophic lateral sclerosis family. *Ann. Neurol.* **49**, 267–271.

Hatayama T., Yamagishi N., Minobe E. and Sakai K. (2001) Role of hsp105 in protection against stress-induced apoptosis in neuronal PC12 cells. *Biochem. Biophys. Res. Commun.* **288**, 528–534.

Hylander B. L., Chen X., Graf P. C. and Subjeck J. R. (2000) The distribution and localization of hsp110 in brain. *Brain Res.* **869**, 49–55.

Ishihara K., Yamagishi N., Saito Y., Adachi H., Kobayashi Y., Sobue G., Ohtsuka K. and Hatayama T. (2003) Hsp105alpha suppresses the aggregation of truncated androgen receptor with expanded CAG repeats and cell toxicity. *J. Biol. Chem.* **278**, 25 143–25 150.

Jensen O. N., Podtelejnikov A. and Mann M. (1996) Delayed extraction improves specificity in database searches by matrix-assisted laser desorption/ionization peptide maps. *Rapid Commun. Mass Spectrom.* **10**, 1371–1378.

Johnston J. A., Dalton M. J., Gurney M. E. and Kopito R. R. (2000) Formation of high molecular weight complexes of mutant Cu, Zn-superoxide dismutase in a mouse model for familial amyotrophic lateral sclerosis. *Proc. Natl Acad. Sci. USA* **97**, 12 571–12 576.

Jonsson P. A., Ernhill K., Andersen P. M., Bergemalm D., Brannstrom T., Gredal O., Nilsson P. and Marklund S. L. (2004) Minute quantities of misfolded mutant superoxide dismutase-1 cause amyotrophic lateral sclerosis. *Brain* **127**, 73–88.

Kato S., Takikawa M., Nakashima K., Hirano A., Cleveland D. W., Kusaka H., Shibata N., Kato M., Nakano I. and Ohama E. (2000) New consensus research on neuropathological aspects of familial amyotrophic lateral sclerosis with superoxide dismutase 1 (SOD1) gene mutations: inclusions containing SOD1 in neurons and astrocytes. *Amyotroph. Lateral Scler. Other Motor Neuron Disord.* **1**, 163–184.

Katsuno M., Sang C., Adachi H., Minamiyama M., Waza M., Tanaka F., Doyu M. and Sobue G. (2005) Pharmacological induction of heat-shock proteins alleviates polyglutamine-mediated motor neuron disease. *Proc. Natl Acad. Sci. USA* **102**, 16 801–16 806.

Kieran D., Kalmar B., Dick J. R., Riddoch-Contreras J., Burnstock G. and Greensmith L. (2004) Treatment with arimoclomol, a coinducer of heat shock proteins, delays disease progression in ALS mice. *Nat. Med.* **10**, 402–405.

Kostic V., Gurney M. E., Deng H. X., Siddique T., Epstein C. J. and Przedborski S. (1997) Midbrain dopaminergic neuronal degeneration in a transgenic mouse model of familial amyotrophic lateral sclerosis. *Ann. Neurol.* **41**, 497–504.

Lee-Yoon D., Easton D., Murawski M., Burd R. and Subjeck J. R. (1995) Identification of a major subfamily of large hsp70-like proteins through the cloning of the mammalian 110-kDa heat shock protein. *J. Biol. Chem.* **270**, 15 725–15 733.

Liu J., Shinobu L. A., Ward C. M., Young D. and Cleveland D. W. (2005) Elevation of the Hsp70 chaperone does not effect toxicity in mouse models of familial amyotrophic lateral sclerosis. *J. Neurochem.* **93**, 875–882.

Maatkamp A., Vlug A., Haasdijk E., Troost D., French P. J. and Jaarsma D. (2004) Decrease of Hsp25 protein expression precedes degeneration of motoneurons in ALS-SOD1 mice. *Eur. J. Neurosci.* **20**, 14–28.

McCarty J. S., Buchberger A., Reinstein J. and Bukau B. (1995) The role of ATP in the functional cycle of the DnaK chaperone system. *J. Mol. Biol.* **249**, 126–137.

Miyazaki K., Fujita T., Ozaki T. *et al.* (2004) NEDL1, a novel ubiquitin-protein isopeptide ligase for dishevelled-1, targets mutant superoxide dismutase-1. *J. Biol. Chem.* **279**, 11 327–11 335.

Niwa J., Ishigaki S., Hishikawa N., Yamamoto M., Doyu M., Murata S., Tanaka K., Taniguchi N. and Sobue G. (2002) Dorfin ubiquitylates mutant SOD1 and prevents mutant SOD1-mediated neurotoxicity. *J. Biol. Chem.* **277**, 36 793–36 798.

Oeda T., Shimohama S., Kitagawa N., Kohno R., Imura T., Shibasaki H. and Ishii N. (2001) Oxidative stress causes abnormal accumulation of familial amyotrophic lateral sclerosis-related mutant SOD1 in transgenic Caenorhabditis elegans. *Hum. Mol. Genet.* **10**, 2013–2023.

Oh H. J., Chen X. and Subjeck J. R. (1997) Hsp110 protects heat-denatured proteins and confers cellular thermoresistance. *J. Biol. Chem.* **272**, 31 636–31 640.

Oh H. J., Easton D., Murawski M., Kaneko Y. and Subjeck J. R. (1999) The chaperoning activity of hsp110. Identification of functional domains by use of targeted deletions. *J. Biol. Chem.* **274**, 15 712–15 718.

Okado-Matsumoto A. and Fridovich I. (2002) Amyotrophic lateral sclerosis: a proposed mechanism. *Proc. Natl Acad. Sci. USA* **99**, 9010–9014.

Parton M. J., Andersen P. M., Broom W. J. and Shaw C. E. (2001) Compound heterozygosity and variable penetrance in SOD1 amyotrophic lateral sclerosis pedigrees. *Ann. Neurol.* **50**, 553–554.

Raviol H., Sadlish H., Rodriguez F., Mayer M. P. and Bukau B. (2006) Chaperone network in the yeast cytosol: Hsp110 is revealed as an Hsp70 nucleotide exchange factor. *EMBO J.* **25**, 2510–2518.

Rudiger S., Buchberger A. and Bukau B. (1997) Interaction of Hsp70 chaperones with substrates. *Nat. Struct. Biol.* **4**, 342–349.

Senderek J., Krieger M., Stendel C. *et al.* (2005) Mutations in SIL1 cause Marinesco-Sjogren syndrome, a cerebellar ataxia with cataract and myopathy. *Nat. Genet.* **37**, 1312–1314.

Shinder G. A., Lacourse M. C., Minotti S. and Durham H. D. (2001) Mutant Cu/Zn-superoxide dismutase proteins have altered solubility and interact with heat shock/stress proteins in models of amyotrophic lateral sclerosis. *J. Biol. Chem.* **276**, 12 791–12 796.

Urushitani M., Kurisu J., Tateno M., Hatakeyama S., Nakayama K., Kato S. and Takahashi R. (2004) CHIP promotes proteasomal degradation of familial ALS-linked mutant SOD1 by ubiquitinating Hsp/Hsc70. *J. Neurochem.* **90**, 231–244.

Vleminckx V., Van Damme P., Goffin K., Delye H., Van Den Bosch L. and Robberecht W. (2002) Upregulation of HSP27 in a transgenic model of ALS. *J. Neuropathol. Exp. Neurol.* **61**, 968–974.

Wang J., Xu G. and Borchelt D. R. (2002a) High molecular weight complexes of mutant superoxide dismutase 1: age-dependent and tissue-specific accumulation. *Neurobiol. Dis.* **9**, 139–148.

Wang J., Xu G., Gonzales V., Coonfield M., Fromholt D., Copeland N. G., Jenkins N. A. and Borchelt D. R. (2002b) Fibrillar inclusions and motor neuron degeneration in transgenic mice expressing superoxide dismutase 1 with a disrupted copper-binding site. *Neurobiol. Dis.* **10**, 128–138.

Wang J., Slunt H., Gonzales V., Fromholt D., Coonfield M., Copeland N. G., Jenkins N. A. and Borchelt D. R. (2003) Copper-binding-site-null SOD1 causes ALS in transgenic mice: aggregates of non-native SOD1 delineate a common feature. *Hum. Mol. Genet.* **12**, 2753–2764.

Watanabe M., Dykes-Hoberg M., Culotta V. C., Price D. L., Wong P. C. and Rothstein J. D. (2001) Histological evidence of protein aggregation in mutant SOD1 transgenic mice and in amyotrophic lateral sclerosis neural tissues. *Neurobiol. Dis.* **8**, 933–941.

Yamagishi N., Ishihara K., Saito Y. and Hatayama T. (2003) Hsp105 but not Hsp70 family proteins suppress the aggregation of heat-denatured protein in the presence of ADP. *FEBS Lett.* **555**, 390–396.

Yasuda K., Nakai A., Hatayama T. and Nagata K. (1995) Cloning and expression of murine high molecular mass heat shock proteins, HSP105. *J. Biol. Chem.* **270**, 29 718–29 723.

Cell

Rac-GAP α-Chimerin Regulates Motor-Circuit Formation as a Key Mediator of EphrinB3/EphA4 Forward Signaling

Takuji Iwasato,[1,*] Hironori Katoh,[2] Hiroshi Nishimaru,[3] Yukio Ishikawa,[2] Haruhisa Inoue,[4] Yoshikazu M. Saito,[1] Reiko Ando,[1] Mizuho Iwama,[1] Ryosuke Takahashi,[4] Manabu Negishi,[2] and Shigeyoshi Itohara[1]

[1]Laboratory for Behavioral Genetics, RIKEN Brain Science Institute (BSI), 2-1 Hirosawa Wako-shi, Saitama 351-0198, Japan

[2]Laboratory of Molecular Neurobiology, Graduate School of Biostudies, Kyoto University, Yoshidakonoe-cho, Sakyo-ku, Kyoto 606-8501, Japan

[3]Neuroscience Research Institute, National Institute of Advanced Industrial Science and Technology (AIST), 1-1-1 Higashi, Tsukuba, Ibaraki 305-8566, Japan

[4]Department of Neurology, Kyoto University Graduate School of Medicine, 54 Kawahara-cho, Shogoin, Sakyo-ku, Kyoto 606-8507, Japan

*Correspondence: iwasato@brain.riken.jp

DOI 10.1016/j.cell.2007.07.022

SUMMARY

The ephrin/Eph system plays a central role in neuronal circuit formation; however, its downstream effectors are poorly understood. Here we show that α-chimerin Rac GTPase-activating protein mediates ephrinB3/EphA4 forward signaling. We discovered a spontaneous mouse mutation, *miffy* (*mfy*), which results in a rabbit-like hopping gait, impaired corticospinal axon guidance, and abnormal spinal central pattern generators. Using positional cloning, transgene rescue, and gene targeting, we demonstrated that loss of α-chimerin leads to *mfy* phenotypes similar to those of *EphA4*$^{-/-}$ and *ephrinB3*$^{-/-}$ mice. α-chimerin interacts with EphA4 and, in response to ephrinB3/EphA4 signaling, inactivates Rac, which is a positive regulator of process outgrowth. Moreover, downregulation of α-chimerin suppresses ephrinB3-induced growth cone collapse in cultured neurons. Our findings indicate that ephrinB3/EphA4 signaling prevents growth cone extension in motor circuit formation via α-chimerin-induced inactivation of Rac. They also highlight the role of a Rho family GTPase-activating protein as a key mediator of ephrin/Eph signaling.

INTRODUCTION

Ephrins are cell-surface-bound ligands for Eph receptors, which comprise the largest family of receptor tyrosine kinases (Eph Nomenclature Committee, 1997). The ephrin/Eph interaction induces bidirectional signaling: ephrin → Eph forward and Eph → ephrin reverse (Noren and Pasquale, 2004; Palmer and Klein, 2003). Ephrin/Eph signaling, which functions in short-range cell-to-cell communication primarily through repulsive effects, is central to neuronal circuit development (Flanagan and Vanderhaeghen, 1998; Palmer and Klein, 2003; Pasquale, 2005).

Downstream signaling has been studied mostly through in vitro cell culture experiments. Particularly important players in both forward and reverse signaling are the Rho-family GTPases (Rho-GTPases), such as RhoA, Rac, and Cdc42, which are the key regulators of actin dynamics (Etienne-Manneville and Hall, 2002; Luo, 2000; Noren and Pasquale, 2004; Wahl et al., 2000). Rho-GTPases are directly activated by Rho-guanine nucleotide-exchange factors (Rho-GEFs) and are inactivated by Rho-GTPase-activating proteins (Rho-GAPs). Accumulating evidence suggests that ephrin/Eph regulates Rho-GTPases through Rho-GEFs (Cowan et al., 2005; Irie and Yamaguchi, 2002; Murai and Pasquale, 2005; Ogita et al., 2003; Penzes et al., 2003; Shamah et al., 2001; Tanaka et al., 2004).

Among the numerous Rho-GEFs involved in ephrin/Eph signaling, ephexin1 is the best characterized. EphA receptors are thought to regulate growth cone dynamics through ephexin1 in axon guidance (Sahin et al., 2005; Shamah et al., 2001). Activation of RhoA induces growth cone retraction and/or collapse, while activated Rac and Cdc42 promote its extension (Etienne-Manneville and Hall, 2002; Luo, 2000). The engagement of Ephs by ephrin leads to activation of the GEF activity of ephexin1 toward RhoA, thereby causing growth cone collapse in vitro (Shamah et al., 2001). However, as *ephexin1*-knockout (KO) mice are apparently normal (Sahin et al., 2005), the role of ephexin1 remains largely unknown. It is also noteworthy that, compared with the considerable attention given to Rho-GEFs, the possible contribution of Rho-GAPs in actin dynamics controlled by ephrin/Eph signaling has largely been neglected.

The roles of ephrin/Eph signaling in vivo have been studied using mouse reverse genetics. An extremely well-characterized case is ephrinB3 → EphA4 forward signaling. *EphrinB3*$^{-/-}$ and *EphA4*$^{-/-}$ mice both display several neural phenotypes, including a rabbit-like hopping gait and impairment of two major motor circuits: the corticospinal tract (CST) and the spinal neuronal circuit controlling locomotion, which is also known as the central pattern generator (CPG). Similar phenotypes are also displayed by *EphA4*$^{KD/KD}$ and *EphA4*$^{FF/FF}$ mice, both of which have impaired kinase activity of EphA4, but not by mice expressing a truncated form of ephrinB3 lacking its cytoplasmic domain (Dottori et al., 1998; Kullander et al., 2003, 2001a, 2001b; Yokoyama et al., 2001). Thus, it is apparent that ephrinB3 → EphA4 forward signaling, but not EphA4 → ephrinB3 reverse signaling, is essential for the formation of these motor circuits.

CST axons controlling voluntary movements arise in the motor cortex, cross into the contralateral side of the medulla, and enter the spinal cord (Gianino et al., 1999; Liang et al., 1991). In wild-type (WT) mice, they rarely cross back to the other side in the spinal cord because ephrinB3 is anchored at the midline and generates repulsive signals through EphA4 receptors expressed on the surface of the CST axon membranes. In *ephrinB3* or *EphA4* mutant mice, due to a lack of repulsive ephrinB3/EphA4 forward signaling, many CST axons fail to stop at the midline and recross it (Kullander et al., 2001a; Yokoyama et al., 2001). Spinal CPGs are thought to generate the repetitive sequential stepping of limbs during walking (Grillner and Wallen, 1985). Locomotor-like rhythmic activity, alternating between the left and right sides, can be evoked in the isolated spinal cords of WT mice (Nishimaru and Kudo, 2000), whereas the activity of the two sides is synchronous in the spinal cords of *ephrinB3*$^{-/-}$ or *EphA4*$^{-/-}$ mice (Kullander et al., 2003). Aberrant midline crossing of axons from EphA4-expressing CPG interneurons is thought to be responsible for the CPG abnormality in *ephrinB3*$^{-/-}$ and *EphA4*$^{-/-}$ mice (Kiehn and Kullander, 2004; Kullander et al., 2003).

The current study provides both in vivo and in vitro evidence that the Rac-specific GAP α-chimerin plays a critical role in the formation of CST and CPGs as an essential downstream component of ephrinB3/EphA4 forward signaling.

RESULTS

A Novel Spontaneous Autosomal Recessive Mutation leading to a Rabbit-like Hopping Gait

We unexpectedly discovered mutant mice with a rabbit-like gait while generating mice homozygous for a ChAT-Cre#23 construct (Inoue et al., 2003). This mutation, which we designated as *miffy* (*mfy*), was autosomal recessive. We initially assumed that *mfy* was caused by gene disruption during transgene integration. However, this was not the case because the *mfy* locus segregated from the transgene, suggesting that the mutation arose spontaneously. *mfy/mfy* mice appeared in crosses at the expected Mendelian frequency and were healthy and fertile. Their bodies were slightly smaller than their littermate controls during the postnatal developmental period. For instance, on postnatal day 10 (P10), the average body weights ± standard error of the mean (SEM) were 4.68 ± 0.17 g, 5.68 ± 0.17 g, and 5.80 ± 0.15 g for the *mfy/mfy* (n = 10), *mfy/+* (n = 12), and +/+ (n = 5) pups, respectively. However, these differences were not evident in adulthood.

WT and *mfy/+* mice moved with a normal alternate step gait. By contrast, all of the *mfy/mfy* mice (n > 100) tended to move their left and right hind limbs synchronously, resulting in a rabbit-like hopping gait (Figure 1A). The mean ± SEM proportion of left-right synchronized gaits among 40 randomly selected gaits was 0 for *mfy/+* (n = 13) and 98.42% ± 0.61% for *mfy/mfy* (n = 19) mice ($p < 0.0001$, unpaired t test). The gross morphology of the *mfy/mfy* mouse brain was indistinguishable from that of its littermate controls (WT and *mfy/+* mice; Figures S1A and S1B). By contrast, a morphological analysis of cross-sections of the spinal cord of *mfy/mfy* mice revealed that the white matter in the dorsal funiculus was reduced, most prominently at the lumbar levels (Figure S1C).

Aberrant Recrossing of CST Axons at the Midline of the Spinal Cord in *mfy/mfy* Mice

The CST axons control voluntary movements through direct or indirect contact with spinal motor neurons (Liang et al., 1991). To visualize these axons, we injected anterograde tracer into the left motor cortex and stained the projections of the CST axons in the medulla and spinal cord. CST axons arising in the left motor cortex crossed to the right side of the medulla in both *mfy/mfy* and control mice (Figure S1D). However, in the spinal cord of control mice (n = 11), CST axons projected only into the contralateral (right) gray matter and barely recrossed the midline into the ipsilateral gray matter, whereas we observed aberrant midline recrossing of these axons in all of the preparations of *mfy/mfy* mouse spinal cords examined (n = 7; Figures 1B and 1C).

To confirm the anterograde tracing results, we injected a retrograde tracer unilaterally into the lumber spinal cord (Figure 1D). In WT mice, most of the retrograde-labeled CST neurons were located in layer V of the contralateral motor cortex (Figure 1E). However, in *mfy/mfy* mice, the ipsilateral cortex also contained many labeled neurons (Figure 1F). Cell-count analyses of the motor cortex revealed that the ipsilateral cortex of WT (n = 4) and *mfy/mfy* (n = 7) mice contained 2.02% ± 0.92% and 34.26% ± 5.22% times as many labeled cells as the contralateral cortex, respectively, which was statistically significant ($p < 0.002$; Figure 1G).

Abnormal CPGs in the Spinal Cord of *mfy/mfy* Mice

To examine the locomotor CPGs underlying limb movements during walking, we isolated the spinal cords from newborn (P1–P3) *mfy/mfy* and control (*mfy/+* and WT) mice and induced locomotor-like activity by applying

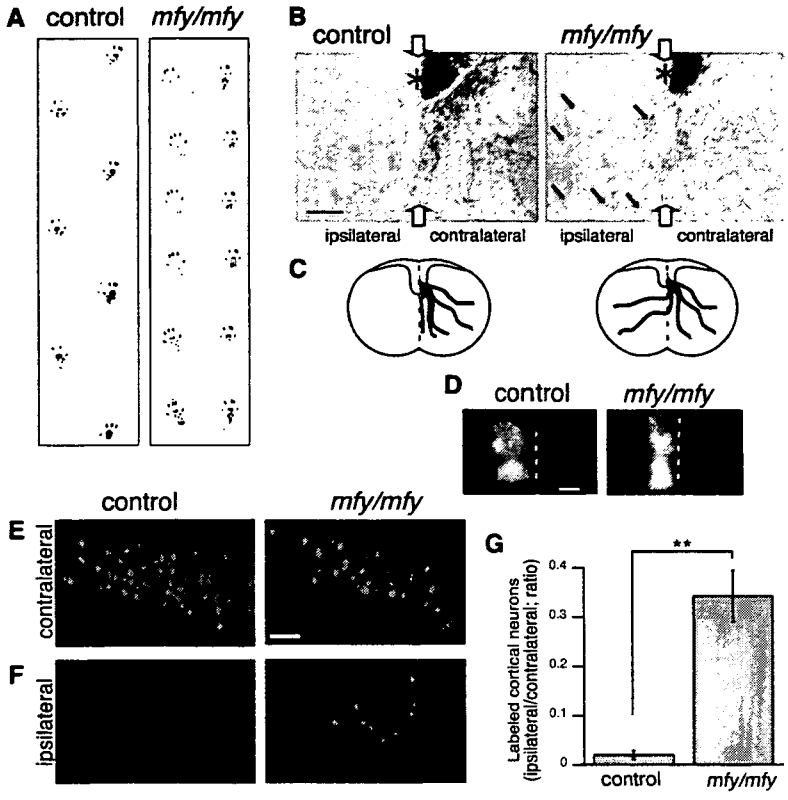

Figure 1. Abnormal Walking and CST Axon Guidance in the Novel Spontaneous Mutant *mfy*

(A) Representative hind-limb footprint patterns. Hind limbs were painted with black ink, and the mice were placed on white paper.

(B) Anterograde tracings of CST axons by biotinylated dextran amine (BDA) and sectioning at cervical levels of the spinal cord. CST axons positioned within the dorsal funiculus (asterisk) on the contralateral side to the tracer injection projected into the spinal gray matter in both control and *mfy/mfy* mice; however, in the *mfy/mfy* mice only, many of the CST axons (blue arrows) recrossed the midline (white arrows).

(C) Schematics of CST axons (red) in the spinal cord.

(D) A fluorescent retrograde tracer cholera toxin B (CTB) was unilaterally injected into the lumbar spinal cord.

(E and F) In the motor cortex layer V of control (WT) mice, most of the labeled neurons were located in the contralateral side (E). In *mfy/mfy* mice, the ipsilateral side also contained many labeled neurons (F).

(G) The ipsilateral/contralateral ratio of numbers of labeled cortical neurons in *mfy/mfy* mice (n = 7) was significantly higher than that of control mice (n = 4). Data are represented as the mean ± SEM: Student's t test, $p < 0.002$. Scale bars: 100 μm.

N-methyl-D-aspartate (NMDA) and serotonin. The ventral root (VR) activity of lumber 2 (L2) represents flexor muscle activity during locomotion, while that of L5 represents extensor activity (Whelan et al., 2000). In control mice, we observed alternation between the left and right L2s (Figures 2A–2C), whereas the cords of *mfy/mfy* mice displayed a synchronous rhythm of the left and right L2s (Figures 2A–2C). The rhythmic activity of the flexors (L2) and extensors (L5) of each limb alternated in both control and *mfy/mfy* mice spinal cords (Figures 2A–2C). We injected a tracer unilaterally into the ventral side of the spinal cords of P4 *mfy/mfy* and control pups, and we found that more neuronal fibers, presumably derived from ipsilateral-projecting interneurons, crossed the midline in the *mfy/mfy* spinal cords than in the control spinal cords (Figure 2D; for quantitative analyses, see Figures S2A and S2B).

The *mfy* Locus Encodes the Rac-Specific GAP α-Chimerin

To locate the *mfy* locus, we employed microsatellites and single-nucleotide polymorphisms (SNPs) that distinguish between the alleles of two inbred mouse strains, DBA/2 (DBA) and C57BL/6 (B6). The *mfy* mutant was identified and maintained in a pure B6 genetic background. We therefore crossed *mfy/mfy* mice with WT DBA mice and obtained *mfy/+* mice in a B6/DBA F_1 genetic background. By backcrossing these F_1 mice to *mfy/mfy* mice and genotyping the DNA of the 299 backcross progeny, we mapped the *mfy* locus to the region between SNPs *rs13476571* and *rs13459064* on chromosome 2 (Figure S3).

In total, 30 genes are known within this 3.27 Mb interval (Table S1). Among these, 10 genes could be excluded because their KO mouse lines have been previously reported to survive to adulthood, and they do not appear to have hopping gaits (for references, see Table S1). We compared the sizes and transcript levels of the remaining 20 genes in the brains of WT and *mfy/mfy* mice at P5 using the reverse transcription-polymerase chain reaction (RT-PCR) with primer sets amplifying the complementary DNA (cDNA) between the 5′ and 3′ untranslated regions (UTRs) and found that the transcripts of only one gene, the α-chimerin (*α-Chn*) gene, differed in size (Figures 3A and 3B; Table S1). α-chimerin is a Rho-GAP that is specific for the positive regulator of actin polymerization, Rac (Diekmann et al., 1991; Hall et al., 1990, 1993). Recent reports using overexpression and/or small-interfering RNA (siRNA)-mediated knockdown in cultured neurons and/or tissue slices suggest that α-chimerin is involved in regulating dendritic morphology and spine density (Buttery et al., 2006; Van de Ven et al., 2005) as well as semaphorin3A-induced growth cone collapse (Brown et al., 2004). However, the role of α-chimerin in living animals has not yet been defined.

α-Chn has two splice isoforms: α1 and α2 (Hall et al., 1990, 1993). A comparison of the sequences of the *α1-Chn* and *α2-Chn* cDNAs of WT and *mfy/mfy* mice revealed that exon 9 (174 base pairs [bp]) was deleted in the

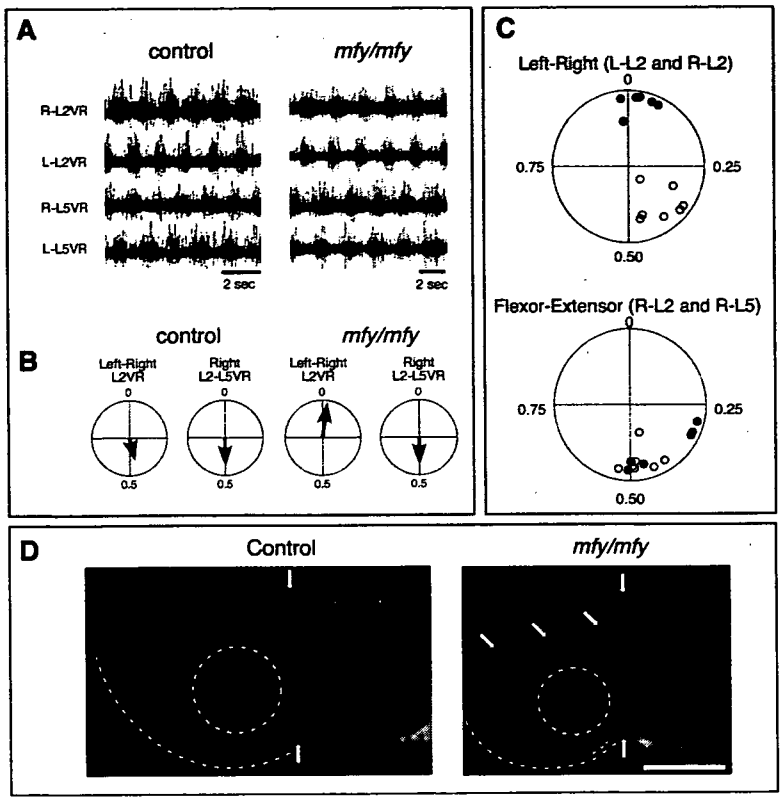

Figure 2. Synchronous Left-Right VR Activity in the Lumbar Spinal Cord of *mfy/mfy* Mice

(A) Locomotor-like motor activity recorded after bath-application of NMDA and serotonin to isolated spinal cords of control and *mfy/mfy* mice. VR activity of the second (L2) and fifth (L5) lumbar segments on the left (L-) and right (R-) sides was recorded using glass-suction electrodes.

(B) Circular phase diagrams for the locomotor-like rhythmic activity of the control and *mfy/mfy* mice shown in (A). Phase relationships between L-L2VR and R-L2VR (left panel) and flexor (R-L2VR) and extensor (R-L5VR) on one side of the lumbar cord (right panel) are indicated in each diagram derived from 30 locomotor cycles. Locomotor cycles in which the two VR activities are in complete alternation have phase values of 0.5. Those that are completely synchronous have phase values of 0 or 1. The mean phase and the r value, which describes the concentration of phase values around the mean, are shown by the direction and magnitude, respectively, of the vector originating from the center of the circle.

(C) Summary plots of seven control (open circles) and six *mfy/mfy* (filled circles) mice at P1–P3.

(D) Transverse spinal cord sections (100 μm thick) at the L2 level after unilateral application of DiI on the ventral side of L4. More neuronal fibers (yellow arrows), which are likely to be derived from ipsilateral-projecting interneurons, crossed the midline (white arrows) to the contralateral (left) side in *mfy/mfy* spinal cords than in control spinal cords. The cell bodies of descending commissural interneurons, shown by dotted circles, were indistinguishable. Scale bar: 500 μm.

$\alpha 1$-*Chn*^{mfy} and $\alpha 2$-*Chn*^{mfy} transcripts (Figure 3A). Exon 9 encodes 58 amino acids, three of which (EIE) are known to be essential for the GAP activity of α-chimerin that inactivates Rac (Ahmed et al., 1994); α2-chimerin^{mfy} was indeed found to lack Rac-GAP activity in vitro (Figure S4). In addition to the α1 and α2 isoforms, we found transcripts of a putative novel isoform that we termed α3 (Figures 3A and 3B). In the $\alpha 3$-*Chn*^{mfy} transcript, four nucleotides (GATG) of exon 9, including the putative initiation codon, were replaced with retroposon sequences, and intron 9 failed to be excised (Figure 3A). The cloning and sequencing of the genomic DNA of the *mfy* allele revealed an insertion of a retroposon into exon 9, which appeared to impair both the donor and the acceptor splicing functions (Figure 3A). Quantitative RT-PCR demonstrated strong $\alpha 2$-*Chn* expression, weak $\alpha 1$-*Chn* expression, and little $\alpha 3$-*Chn* expression in the motor cortex and spinal cord of P4 WT mice (Figure 3C). We therefore focused on the α2 isoform in subsequent studies. We raised an α2-chimerin-specific polyclonal antibody and confirmed by western blot analysis that the α2-chimerin^{WT} protein could not be detected in the *mfy/mfy* brain (Figure 3D). Furthermore, even the α2-chimerin^{mfy} protein was barely detected in the *mfy/mfy* brain and spinal cord (Figures 3D and 3E), suggesting that endogenous α2-chimerin^{mfy} is much less stable in neurons than α2-chimerin^{mfy} overexpressed in cultured cells (Figure S4B).

Improved Locomotor Behavior of *mfy/mfy* Mice Expressing Transgenic *α-Chn*

To confirm that *α-Chn* was the *mfy* gene, we tested whether transgenic (Tg) expression of *α-Chn* rescued the *mfy* phenotype. We modified a bacterial artificial chromosome (BAC) clone that covered the 49 kb upstream region and exons 1–7 of *α-Chn* using Red/ET homologous recombination and flp/FRT recombination in order to make a BAC *α-Chn* construct in which exon 7 was followed by a cDNA encoding exons 8–13 and a poly(A) signal (Figure 4A). We then generated two lines (#539 and #883) of BAC Tg mice by microinjecting the construct into pronuclei and mated them with *mfy/mfy* mice to obtain Tg mice in the *mfy/mfy* background (Figure 4B). There were no improvements in the gaits of the Tg#539:*mfy/mfy* mice (see Figure S5 legend), consistent with no detectable

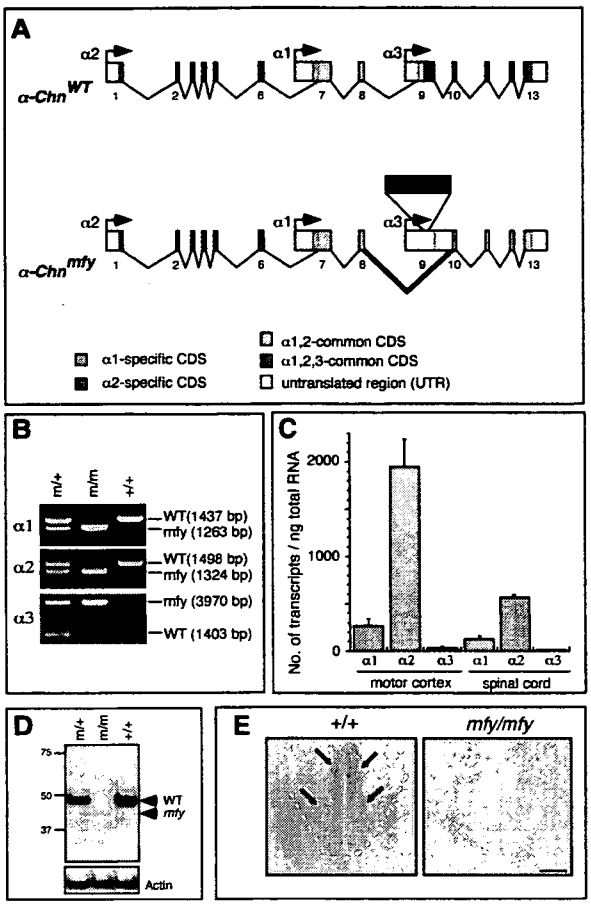

Figure 3. The *mfy* Locus Encodes α-Chimerin Rac-GAP

(A) Schematic exon-intron structures of *α1-Chn*, *α2-Chn*, and *α3-Chn* splicing variants for the WT (*α-Chn*^{WT}) and *mfy* (*α-Chn*^{mfy}) alleles. Retroposon (Tn) insertion into exon 9 in the *mfy* mutant resulted in deletion (red lines) of exon 9 (174 bp) in the *α1* and *α2* transcripts, and deletion of four nucleotides (including the putative initiation codon) and failure of intron 9 splicing in the *α3* transcript. CDS: coding sequences.

(B) RT–PCR products from between the 5′ UTR and the 3′ UTR of the *α1-Chn*, *α2-Chn*, and *α3-Chn* splicing isoforms in cDNAs derived from WT (+/+), *mfy*/+ (m/+), and *mfy/mfy* (m/m) brains at P5. PCR products from the WT and mutant (mfy) *α1-Chn*, *α2-Chn*, and *α3-Chn* isoforms were purified and cloned, and their nucleotide sequences were determined.

(C) *α2-Chn* predominates in the developing motor cortex and spinal cord. Real-time quantitative RT-PCR of *α1-Chn*, *α2-Chn*, and *α3-Chn* in the motor cortex and spinal cord of WT mice at P4. All data are presented as the mean ± SEM (n = 3 mice).

(D) Western blot using an α2-chimerin-specific antibody revealed that α2-chimerin^{WT} protein (WT) was absent from *mfy/mfy* mice. Unexpectedly the mutant protein (mfy) was barely detectable in *mfy*/+ and *mfy/mfy* mice. Total lysates from P10 of the mouse telencephalon were used.

(E) Immunohistochemistry using α2-chimerin-specific antibody revealed strong expression of α2-chimerin in the CST (arrows) of the dorsal funiculus (dotted line) of the WT spinal cord, suggesting that α2-chimerin functions in developing CST axons. α-chimerin was not detectable in *mfy/mfy* spinal cords. Scale bar: 50 μm.

α-chimerin expression in these mice (Figures S5A and S5B). By contrast, considerable improvement was observed in the gaits of the Tg#883:*mfy/mfy* mice (Figure 4C). The average ± SEM proportion of left-right synchronized gaits in 40 randomly selected gaits of Tg#883:*mfy/mfy* mice (n = 13) was 53.65% ± 6.56%, which was substantially less than in their littermate *mfy/mfy* mice (n = 6, 99.58% ± 0.42%; $p < 0.0001$, unpaired t test). α-chimerin protein was expressed at low levels in Tg#883:*mfy/mfy* mice (Figures S5A–S5C), which was consistent with the moderate rescue of gait observed in these mice. These results strongly suggest that *α-Chn* is the causal gene of the *mfy* mutation.

Generation and Characterization of *α-Chn* KO Mice

To further confirm that the *mfy* gene encoded *α-Chn*, we deleted exons 9 and 10 from the allele by a gene-targeting technique in embryonic stem (ES) cells and Cre/loxP recombination in the mouse germline and generated mice homozygous for the targeted allele (*α-Chn* KO mice; Figures 4D and S5D). These mice had a hopping gait similar to that of *mfy/mfy* mice (Figure 4E). They also demonstrated aberrant midline recrossing of CST axons (Figure 4F), aberrant midline crossing of spinal local circuit neurons (Figure S2C), and shorter ventral extension of the dorsal funiculus in the spinal cord (data not shown). Furthermore, they showed abnormal spinal CPGs (Figures 4G and S6). All of these phenotypes were similar to those of *mfy/mfy* mice. Thus, we concluded that the *mfy* phenotypes were caused by *α-Chn* disruption.

Localization of α-Chimerin Proteins in CST

The phenotypes of *mfy/mfy* and *α-Chn* KO mice (hopping gait, Figures 1A and 4E), abnormal spinal-cord morphology (Figure S1C), abnormal CPGs (Figures 2C and 4G), aberrant midline crossing by CPG axons (Figures 2D and S2), and aberrant midline recrossing by CST axons (Figures 1B and 4F) appeared to be identical to those reported for *ephrinB3*$^{-/-}$ and *EphA4*$^{-/-}$ mice (Dottori et al., 1998; Kullander et al., 2003, 2001a; Yokoyama et al., 2001) and for *EphA4*$^{FF/FF}$ and *EphA4*$^{KD/KD}$ mice expressing a mutant EphA4 lacking kinase activity (Kullander et al., 2001b). Nevertheless, the anterior commissure, the formation of which is known to be dependent on EphA4 reverse signaling (Kullander et al., 2001b), appeared normal in *mfy/mfy* mice (Figure S1B). Hence, it seemed likely that the *mfy* phenotype was caused by impairment of ephrinB3/EphA4 forward signaling.

Using immunohistochemistry, we found that α2-chimerin colocalized with EphA4 in the developing CST (Figures S7A and S7C). In *α-Chn* KO CST, α2-chimerin was not detected, but the levels of EphA4 expression appeared to be unaltered (Figures S7B and S7D). We also found that the α2-chimerin protein was present in the growth cones of cultured neurons derived from the anterior dorsomedial to dorsal neocortex (motor cortex; Figure S8C). These results suggest that α-chimerin functions